Interaction of Oppositely Charged Polymer–Surfactant System Based on Surface Tension Measurements

Anis A. Ansari[1], M. Kamil*[,2] and Kabir-ud-Din[3]

[1]University Polytechnic

*[,2] Department of Petroleum Studies

[3]Department of Chemistry

Aligarh Muslim University, Aligarh-202002, U.P., India

[1]anisansari_amu@yahoo.co.in; [2]sm_kamil@rediffmail.com; [3]kabir7@rediffmail.com

Corresponding Author:*E-mail: sm_kamil@rediffmail.com (M. Kamil)

Abstract

The interaction between oppositely charged polymer-surfactant systems has been studied using surface tension measurements wherein the dependence of interaction phenomenon over the presence of anionic polyelectrolyte sodium carboxymethylcellulose (NaCMC) with variation of tail length of cationic surfactants, cetyltrimethylammonium bromide (CTAB), tetradecyltrimethylammonium bromide (TTAB), and dodecyltrimethylammonium bromide (DTAB) was investigated. It is observed that the cationic surfactants induced cooperative binding with the anionic polyelectrolyte at critical aggregation concentration (cac) and the cac values are considerably lower than the corresponding critical micelle concentration (cmc) for each of the surfactant irrespective of their hydrophobic tail size. The cmc of surfactants were observed at slightly higher surfactant concentration in polyelectrolyte solution than that in pure water. It was found that the surfactants with longer tail size strongly favour the interaction with NaCMC, indicating the dependence of aggregation phenomenon on the tail size of the surfactants.

Keywords

Cationic Surfactants, Anionic Polyelectrolyte, Surface Tension, Tail Size

Introduction

The use of mixtures containing surfactant and polymer has been increased many folds in recent years due to their importance in a variety of industrial applications in cosmetics, personal-care products, foods, pharmaceuticals, detergents, and mineral processing [1,2]. In general, polymers are added to the systems to control rheology, stability of the system, or to manipulate surface adsorption. Interactions within the mixture are driven by hydrophobic, dipolar, and electrostatic forces. When surfactants are introduced into a solution containing oppositely charged polymer, strong electrostatic interactions are referred as 'strongly interacting system', as the attractive electrostatic forces are extremely important in the oppositely charged polymer and surfactant [3-5]. There has been significant research work focusing on the interaction of oppositely charged polyelectrolytes and surfactants in recent years [6-24].

Surfactants in the presence of an oppositely charged polyelectrolyte start forming aggregates with the polyelectrolyte when surfactant concentration exceeds its critical aggregation concentration (cac). The aggregation of polyelectrolyte and surfactant with opposite charges greatly depends on the properties of surfactant and polyelectrolyte [21]. Polyelectrolyte–surfactant complex formation originates from electrostatic bonding, and is further stabilized by the hydrophobic interactions of surfactant tails [22]. In this process, the counter ion of the polyelectrolyte is replaced by the surfactant ion, and the binding site of the polyelectrolyte and the surfactant forms a neutral ion pair. The large electrostatic attraction in this association process makes binding extremely favourable, and is dependent on the ionic charge density of the polyelectrolyte. Binding in such systems, therefore, occurs at very low free-surfactant concentration [25]. The conformational properties and the dynamic behaviour of the polyelectrolyte chains are determined by the degree of ionization, and the counter ion concentration and distribution [26]. In aqueous solution the solvation properties and the

hydrophobic interactions are also important that strongly influence the conformational properties of the polymer. The counter ions may be solvated in different ways and hence influence the polymer solvation. Low molecular-weight amphiphiles may either redistribute to the polymer segment region or adsorb the backbone affecting the chemical properties of the polymer [27]. Due to the presence of strong electrostatic interaction in oppositely charged systems [28], the polyelectrolyte gives rise to an uneven distribution of ions in solution and the concentration of counterions is strongly enhanced near the polyelectrolyte which decreases rapidly with distance. The uneven distribution of counterions also applies to monomeric surfactant counterions present in the polyelectrolyte solution. The major reason for cooperative binding of surfactant molecules to an oppositely charged polyelectrolyte is the electrostatic stabilization of the surfactant micelles.

Thalberg and Lindman [29] studied the phase behaviour of systems of polyacrylate and cationic surfactants. The association between homopolymer and surfactant reveals that, at low surfactant concentrations, there is no significant association in any polymer concentration. Above cac, the polymer-bound surfactants increase up to certain surfactant concentration which develops linearly with polymer concentration. Micelle formation of surfactant starts as the surfactant concentration increases further after saturation of polymer chains; at this stage free surfactant micelles and surfactant aggregated polymer coexist in the solution. In the presence of polyelectrolyte, micelle size of surfactants is slightly lower than those of micelles formed in the absence of a polymer in solution. In addition to forming micelles, the surfactant can isolate its hydrophobic groups from the aqueous phase by associating them with the hydrophobic part of the polymer.

Experimental Section

Materials

Cetyltrimethylammonium bromide (CTAB, purity>99.0%) from Merck, Germany, tetradecyltrimethylammonium bromide (TTAB, purity=99.0%) from Sigma Aldrich, USA, dodecyltrimethylammonium bromide (DTAB, purity=99.0%) from TCI Tokyo Kasei Kogyo Co. Ltd., Japan, and sodium carboxymethylcellulose (NaCMC, purity>99.0%, molecular weight=90000, degree of substitution=0.7) from Sigma Aldrich, USA, were used as received for preparation of solutions. Demineralised double-distilled water (specific conductivity~1-10x10^{-6} $S.cm^{-1}$) was used in preparation of solutions throughout the experimentation and sufficient time was given for stabilization.

Method

The surface tension measurements were carried out on a Tensiometer (S. D. Hardson, Kolkata, India), by ring detachment technique in which a ring was submerged into the solution under investigation and then force slowly increased to take up the ring on liquid surface and further to detach the ring from surface film of the solution. The surface tension values (γ) were accurate within $\pm$0.05 $mN.m^{-1}$. Measurements were performed by progressively adding concentrated stock solution of the individual surfactants in the solution. Surface tension data were taken at a time interval of five minutes after stirring the solutions at 30$\pm$1 ^{0}C temperature.

Results and Discussion

The tensiometric plot of CTAB shows a sharp decrease in surface tension with a slight increase in [CTAB] up to cac, then it approximately keeps constant giving 'first plateau' until critical saturation concentration C_s. A further decrease in surface tension is observed up to cmc, beyond which it further stabilizes, giving 'second plateau' due to formation of free micelles in the solution [30]. The plot of CTAB in pure water (Figure 1a) shows only one critical concentration (i.e., at cmc), while in the presence of NaCMC three critical concentrations (first at cac, second at C_s and third at cmc) are observed. This indicates the influence of NaCMC in the solution and its association with the cationic surfactant CTAB. C_s represents the critical saturation concentration of the surfactant (Figure 1b) when all the binding sites on polyelectrolyte are saturated due to adsorption of CTAB over polymer backbone. During this association process (at first plateau), surface tension of the solution is almost constant as the added surfactant get associated with the polyelectrolyte molecules in the solution and surfactant free molecules are not available to affect the surface properties of the solution. Cationic head groups of surfactant individually bind to the anionic carboxylate groups on the polymer chains due to electrostatic attraction. When all the binding sites on polyelectrolyte molecules are saturated with surfactant molecules, surface tension starts decreasing with increase in CTAB concentration further till a certain

concentration, termed as critical micelle concentration (cmc) is reached. At cmc, the micellization of polymer bound surfactant occurs resulting in the formation of insoluble polymer-surfactant complexes. This suggests that the polymer-surfactant system also undergoes a two-stage interaction process where the surfactant binds to the polyelectrolyte due to electrostatic attraction; thereafter, the micellization of polymer-bound surfactant molecules occurs as reported in literature [31-33].

Almost similar trends of surface tension plots were obtained with other surfactants having the same head group but a changed hydrophobic tail (i.e., TTAB and DTAB) (Figures 2 and 3). A significant change in the cmc of the cationic surfactants CTAB, TTAB, and DTAB was observed as represented in Figure 4, which indicates that the cmc found in the presence of NaCMC is higher in comparison to that of the pure water. This is due to the association phenomenon and formation of polymer-surfactant complexes as a result of polymer surfactant interaction. The surface tension values at cmc (γ_{cmc}) plotted in Figure 5 show a less significant variation in the presence of polyelectrolyte, which is in agreement with the literature [3, 31]. Figure 6 shows the schematic illustration of the complex formation after cmc in an oppositely charged polymer-surfactant system in aqueous medium.

Conclusions

The interaction between anionic polyelectrolyte sodium carboxymethylcellulose in aqueous solution with cationic surfactants cetyltrimethylammonium bromide, tetradecyltrimethylammonium bromide, and dodecyltrimethylammonium bromide has been studied using surface tension measurements. It is evident from the results that the cationic surfactants interact strongly with the oppositely charged anionic polymer. The analysis of cac and cmc of cationic surfactants indicates clearly the existence of strong electrostatic interactions of these surfactants with oppositely charged NaCMC. At cac, the surfactant binds to the polymer due to strong electrostatic interactions, and after saturation of the binding sites of the polyelectrolyte at critical saturation concentration, the surface tension decreases further on increasing surfactant concentration until it reaches the cmc of the surfactant. The study of tail size variation on interaction indicates that the surfactants with longer tail size favour the interaction.

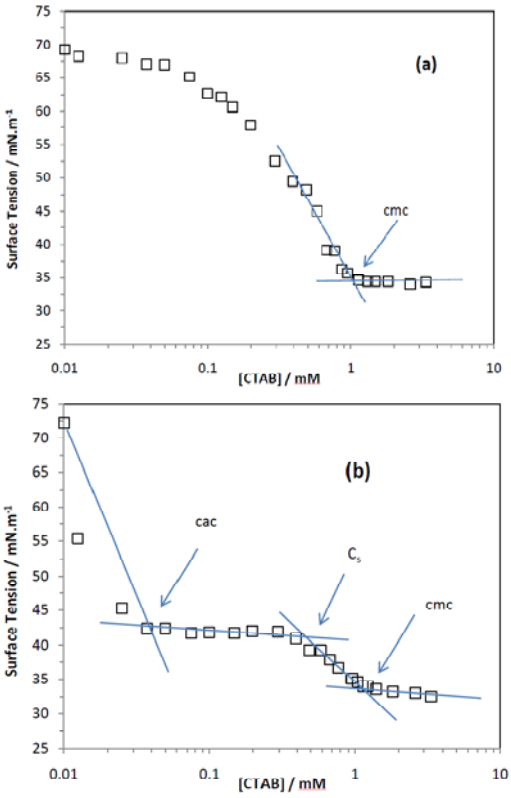

FIG. 1 VARIATION OF SURFACE TENSION (γ) WITH CTAB CONCENTRATION IN PURE WATER (A), AND 0.01 G% NACMC AQUEOUS MEDIUM (B) AT 30 ^{0}C

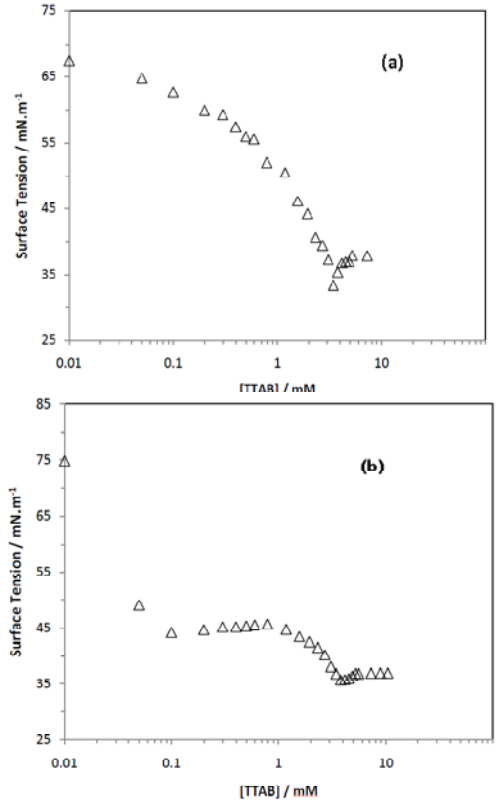

FIG. 2 VARIATION OF SURFACE TENSION (γ) WITH TTAB CONCENTRATION IN PURE WATER (A), AND 0.01 G% NACMC AQUEOUS MEDIUM (B) AT 30 ^{0}C

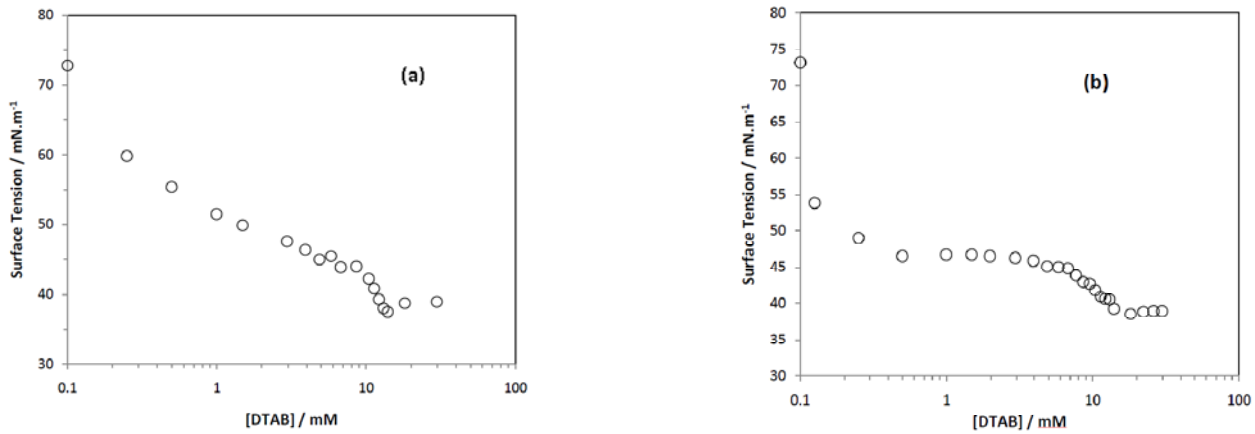

FIG. 3 VARIATION OF SURFACE TENSION (γ) WITH DTAB CONCENTRATION IN PURE WATER (A), AND 0.01 G% NACMC AQUEOUS MEDIUM (B) AT 30 ^{0}C

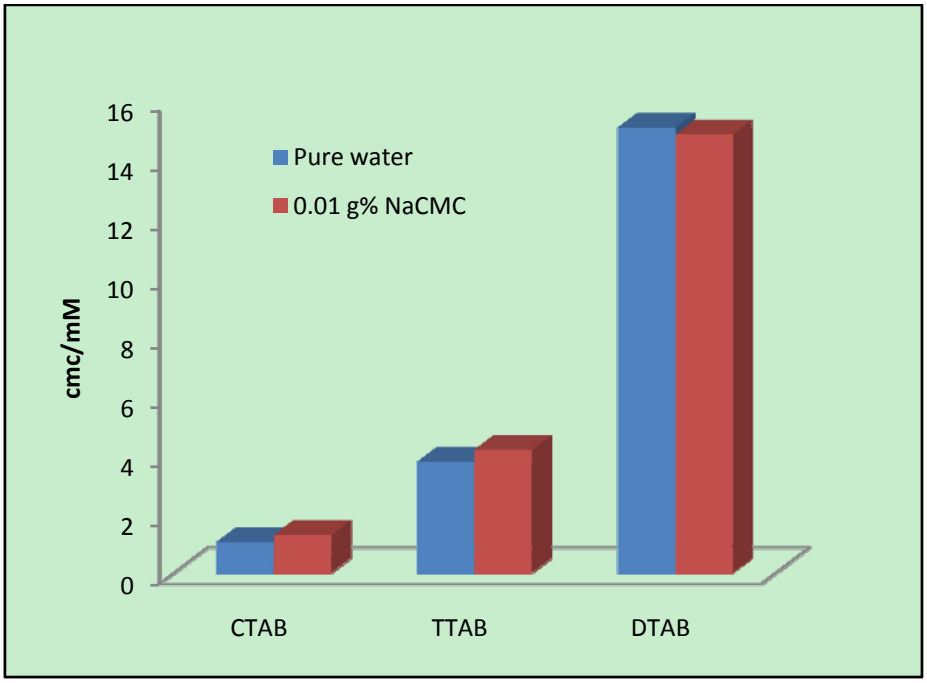

FIG. 4 COMPARISON OF CRITICAL MICELLE CONCENTRATION (CMC) OF CTAB, TTAB, AND DTAB IN PURE WATER AND IN POLYELECTROLYTE SOLUTION AT 30 ^{0}C (BASED ON SURFACE TENSION MEASUREMENTS)

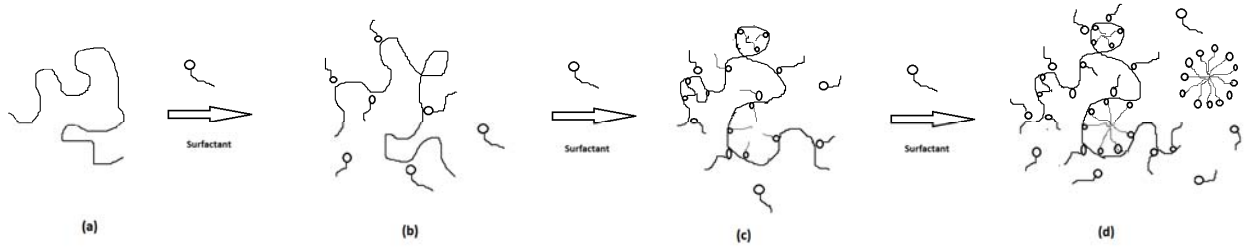

FIG. 6 SCHEMATIC ILLUSTRATION OF POLYELECTROLYTE CHAIN (A), POLYMER SURFACTANT ASSOCIATION (B), BOUND-SURFACTANT MOLECULES AFTER CAC (C), AND COMPLEX FORMATION AFTER CMC (D) IN AN OPPOSITELY CHARGED POLYMER-SURFACTANT SYSTEM IN AQUEOUS MEDIUM

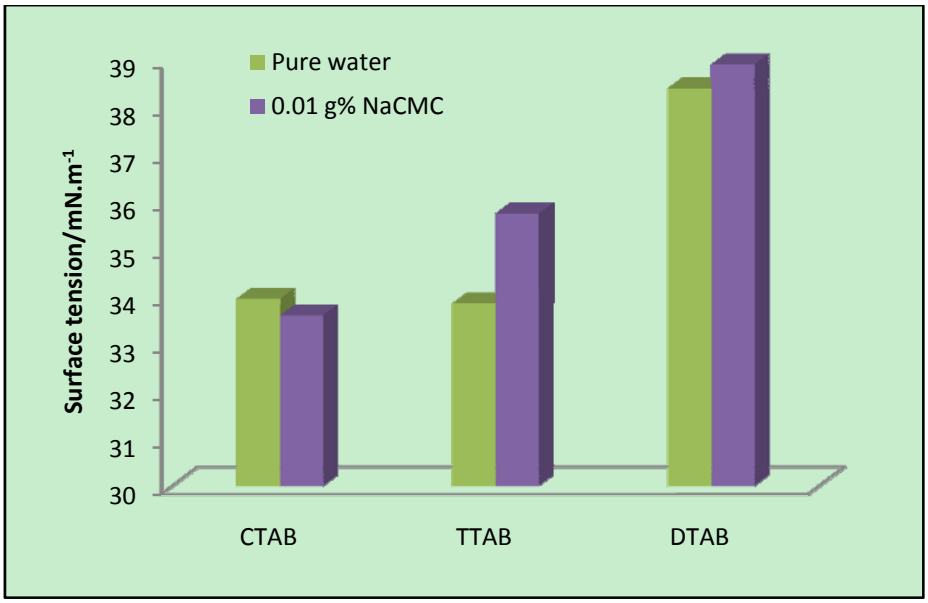

FIG. 5 COMPARISON OF SURFACE TENSION AT CMC (γ_{CMC}) OF CTAB, TTAB, AND DTAB IN PURE WATER AND IN POLYELECTROLYTE SOLUTION AT 30 ^{0}C (BASED ON SURFACE TENSION MEASUREMENTS)

REFERENCES

[1] E. D. Goddard and K. P. Ananthapadmanabhan, *Interactions of Surfactants with Polymers and Proteins*, CRC Press: Boca Raton, 1993.I. A. Ivanov, I. P. Kamenova, V. T. Georgieva, E. B. Kamenska and G. S. Georgiev, Mixed surfactant –polyzwitterion self-assemblies in aqueous solutions, *Colloids Surf. A*, 282, 129-133, 2006.

[2] C. G. Bell, C. J. W. Breward, P. D. Howell, J. Penfold and R. K. Thomas, Polymer-surfactant macroscopic modeling of the surface tension, *Langmuir*, 23, 6042-6052, 2007.

[3] J. C. T. Kwak, *Polymer-Surfactant Systems*, Marcel Dekker: NewYork, 1998.

[4] H. Morawetz, *Macromolecules in Solution*, John Wiley & Sons: New York, 1975.

[5] N. Plucktaveesak, A. J. Konop and R. H. Colby, Viscosity of polyelectrolyte solutions with oppositely charged surfactant, *J. Phys. Chem. B*, 107, 8166-8171, 2003.

[6] K. Kogej, Fluorescence and conductivity studies of polyelectrolyte-induced aggregation of alkyltrimethylammonium bromides, *Langmuir*, 15, 4251-4258, 1999.

[7] B. Lindman, K. Thalberg, E. D. Goddard and K. P. Ananthapadamanabham, in *Interaction of Surfactants with Polymers and Proteins*, CRC Press: Boca Raton, 1993.

[8] P. Hansson and B. Lindman, Surfactant-polymer interaction, *Curr. Opin. Colloid Interface Sci.*, 1, 604-613, 1996.

[9] H. H. Schwarz, K. Richau and R. Apostel, The combination of ionic surfactants with polyelectrolytes- A new material for membranes, *Macromol. Symp.*, 126, 95-104, 1997.

[10] I. Satake and J. T. Yang, Interaction of sodium decyl sulfate with poly(L-ornithine) and poly(L-lysine) in aqueous solution, *Biopolymers*, 15, 2263-2275, 1976.

[11] K. Hayakawa and J. C. T. Kwak., Study of surfactant – polyelectrolyte interactions 2. Effect of multivalent counter ions on the binding of dodecyltrimethylammonium ions by sodium dextran sulphate and sodium poly(styrene sulfonate) in aqueous solution, *J. Phys. Chem.*, 87, 506-509, 1983.

[12] A. Malovikova, K. Hayakawa and J.C.T. Kwak, Study of surfactant polyelectrolyte interactions 4. Surfactant chain length dependence of the binding of alkyl pyridinium cations to dextran sulphate, *J. Phys. Chem.*, 88, 1930-1933, 1984.

[13] J. Skerjanc, K. Kogej and G. Vesnaver, Polyelectrolyte surfactant interaction: Enthalpy of binding of dodecyl and cetyl pyridinium cations to poly(styrene sulfonate) anions, *J. Phys. Chem.*, 92, 6382-6385, 1982.

[14] J. Skerjanc and K. Kogej, Thermodynamic and transport properties of polyelectrolyte-surfactant complex solution at various degrees of complexation, *J. Phys. Chem.*, 93, 7913-7915, 1989.

[15] M. Almgren, P. Hansson, E. Mukhtar and J. V. Stam, Aggregation of alkyl trimethylammonium surfactants in aquous poly(styrene sulphonate) solutions, *Langmuir*, 8, 2405-2412, 1992.

[16] F. M. Winnik and S. T. Regismond, Fluorescence methods in study of interaction of surfactants with polymers, *Colloid Surf. A*, 118, 1-39, 1996.

[17] K. Hayakawa, J. C. T. Kwak and D. N. Holland, *Cationic Surfactants: Physical Chemistry*, Marcel Dekker: New York, 1991.

[18] I. Linch, J. Sjostrom and L. Piculell, Reswelling of polyelectrolyte hydrogels by oppositely charged surfactants, *J. Phys. Chem. B*, 109, 4258-4262, 2005.

[19] Y. Li, P. L. Dubin and C. A. Herb, Structure and flow in surfactant solutions, *ACS Symposium Series*, 578, American Chemical Society: Washington DC, 1994.

[20] M. Vincekovic, M. Bujan, I. Smit and N. Filipovic-Vincekovic, Phase behavior in mixtures of cationic surfactant and anionic polyelectrolytes, *Colloid Surf. A: Physicochem. Eng. Aspects*, 255, 181-191, 2005.

[21] D. F. Anghel, F. M. Winnik and N. Galatanu, Effect of the surfactant head group length on the interactions between polyethylene glycol mono-nonylphenyl ethers and poly(acrylic acid), *Colloid Surf. A: Physicochem. Eng. Aspects*, 149, 339-345, 1999.

[22] G. Bai, M. Nichifor, A. Lopes and M. Bastos, Thermodynamics of self assembling of hydrophobically modified cationic polysaccharides and their mixtures with oppositely charged surfactants in aqueous solution, *J. Phys. Chem. B*, 109, 21681-21689, 2005.

[23] B. Magny, I. Iliopoulos, R. Zana and R. Audebert, Mixed micelles formed by cationic surfactants and anionic hydrophobically modified polyelectrolytes, *Langmuir*, 10, 3180-3187, 1994.

[24] M. S. Bakshi and S. Sachar, Surfactant polymer interactions between strongly interacting cationic surfactants and anionic polyelectrolytes from conductivity and turbidity measurements, *Colloid Polymer Sci*., 282, 993–999, 2004.

[25] L. Wang and H. Yu, Chain conformation of linear polyelectrolyte in salt solutions: sodium poly(styrenesulfonate) in potassium chloride and sodium chloride, *Macromolecules*, 21, 3498-3501, 1998.

[26] A. Herslof and L. O. Sundelof, Interaction between polyelectrolyte and surfactant of opposite charge: Hydrodynamic effects in the sodium hyaluronate/tetradecyltrimethylammonium bromide/sodium chloride/water system, *J. Phys. Chem.*, 96, 2345-2348, 1992.

[27] P. Dev, N. Dev, P. Somasundaran, A. Moscatelli, S. Jockusch, N. J. Turro, K.P. Ananthapadamanabham and M. F. Ottaviani, Interactions of a hydrophobically modified polymer with oppositely charged surfactants, *Langmuir*, 23, 5906-5913, 2007.

[28] K. Thalberg and B. Lindman, Phase behavior of systems of polyacrylate and cationic surfactants, *Langmuir*, 7, 2893-2898, 1991.

[29] Q. Wu, M. Du, Y. Shangguan, J. Zhou and Q. Zheng, Investigation on the interaction between CTAB and NaCMC in semidilute aqueous solution based on rheological measurement, *Colloid Surf. A: Physicochem. Eng. Aspects*, 332, 13–18, 2009.

[30] C. Wang and K. C. Tam, New insights on the interaction mechanism within oppositely charged polymer/ surfactant systems, *Langmuir*, 18, 6484-6490, 2002.

[31] T. Chakraborty, I. Chakraborty and S. Ghosh, Sodium carboxymethylcellulose-CTAB interaction: A detailed thermodynamic study of polymer-surfactant interaction with opposite charges, *Langmuir*, 22, 9905-9913, 2006.

[33] N. Sardar, M. Kamil and Kabir-ud-Din, Interaction between nonionic polymer hydroxypropyl methyl cellulose (HPMC) and cationic gemini/conventional surfactants, *Ind. Eng.Chem. Res.* 51, 1227−1235, 2012.

Author Biographies

[1]**Anis A. Ansari** is Assistant Professor in the University Polytechnic, Aligarh Muslim University, India since 2004. He has received his Bachelor Degree in Chemical Technology (Plastics) from Harcourt Butler Technological Institute, Kanpur, India and Master Degree in Petroleum Processing and Petrochemical Engineering from the Aligarh Muslim University. His research interests are Polymer –Surfactant Interactions, conducting polymers, and polymer blends.

[2]**M. Kamil** is currently a Professor at Aligarh Muslim University, India. He received his M.E. degree from IIT Roorkee (formerly University of Roorkee), and Ph.D. from the Aligarh Muslim University, India. His research interests are Polymer –Surfactant Interactions, Synthesis of STF and Process heat transfer.

[3]**Kabir-ud-Din** is currently a UGC-BSR Faculty Fellow at Aligarh Muslim University, Aligarh, India. He has been a Professor of Physical Chemistry at the same university since 1993. He received his M.Sc. and Ph.D. degrees from. Aligarh Muslim University, Aligarh. He held post-doctoral positions at Prague (Czech Republic), Keele (UK), and Austin (USA). His research interests are in micellar catalysis, kinetics, electrochemistry, amphiphilic systems, and so on.

Quenching and Heat Transfer Properties of Aged and Unaged Vegetable Oils

Ester C. de Souza*[1], Luiz F. O. Friedel[2], George E. Totten[3], Lauralice C. F. Canale[4]

Universidade de São Paulo, Escola de Engenharia de São Carlos, São Carlos, SP, Brazil
Texas A&M University, Department of Mechanical Engineering, College Station, Texas, USA

* [1]esterfisica@yahoo.com.br; [2]lf.nando@yahoo.de; [3]lfcanale@sc.usp.br; [4]GETotten@aol.com

Abstract

Vegetable oils may be potentially used as an alternative basestocks to petroleum oil for the formulation of quenchants. Comparative performance cooling curve of a number of vegetable oil basestocks commercially available in Brazil was reported previously. These basestocks included: soybean, canola, corn, cottonseed and sunflower oils. However, these particular vegetable oils exhibit very poor thermal-oxidative stability, relative to petroleum oil, which is attributable to their molecular composition. To address this specific deficiency which affects long-term performance, a number of additional vegetable oils with much more favorable molecular structure were examined including: peanuit (groundnut) oil and coconut oil. To assess the quenching performance compared to conventional and accelerated quenching oils, cooling curve performance according to ASTM D6200 for two bath temperatures (60 °C and 90 °C) was determined. In addition, effective heat transfer coefficients were calculated and compared. It is noteworthy that the vegetable oils evaluated did not exhibit classical film boiling or nucleate boiling behavior during quenching.

Keywords

Quench; Vegetable Oil; Heat Transfer; Oxidative Stability; Cooling Curve

Introduction

The most common used quenchants is water. However, petroleum oil (mineral oil) derived quenchants are used when lower cooling rates and more uniform cooling is desired for better distortion control and crack prevention of alloy steels. However, petroleum oil possesses a number of significant disadvantages including: 1) poor biodegradability (Jones, 1996), 2) toxicity (Henry, 1998), 3) flammability and 4) petroleum oil is not a renewable basestock (Erdman, 1998). Therefore, it is of continuing interest to identify a viable alternative to petroleum oil as a basestock for industrial oil formulation such as quenchants for heat treating applications (Erdman, 1998).

Currently vegetable oils are one of the most commonly identified alternative basestocks to petroleum oils primarily because they are biodegradable and are obtained from renewable sources. Brazil has shown interest in the behavior of soybean oil for use as coolants (and quenchants) and for lubrication formulation because it is a biodegradable renewable basestock and it represents 95% of all seed oil production in the country (Otero, 2011 and Souza, 2009). Soybean oil has shown excellent performance in various commercial applications (Souza, 2011). However, its oxidative instability and its narrow viscosity range substantially limits its use as a quenchant.

While palm oil (dende oil) occupies a prominent position on the world market, it is the second most produced seed oil behind only soybean oil, it is not currently produced at a high level in Brazil. Relative to soybean oil, palm oil contains a substantially higher saturated fatty ester content and significantly lower polyunsaturated acid content in the overall triglyceride structure of the two seed oils and is therefore more resistant to oxidation. This is because molecular double bonds, especially double bonds in conjugation which are in greater concentration in vegetable oils such as soybean oil, react more easily with oxygen to form free radicals leading to faster degradation when subjected to elevated temperatures as would be encountered during quenching of steel. Recently, it has been shown that, as expected, palm oil is significantly more oxidatively stable than soybean oil but still not as stable as petroleum oil (Belinato, 2011).

The objective of this work is to continue these studies by evaluating peanut oil and coconut oil. Peanut oil is often

used as the choise of vegetable oil for deep frying in the food preparation industry because of its higher smoke point and better thermal-oxidative stability (Tan, 2002). Coconut oil was selected because it contains an even greater amount of saturated fatty esters and lower degree of unsaturation in its triglyceride composition than any of the vegetable oils evaluated in these studies to date [5,8]. The results of oxidative stability testing and cooling curve comparison will be reported here.

Experimental Methods and Materials

The vegetable oils used for this work were purchased at the local market in São Carlos, São Paulo, Brazil, and were used in the as-purchased condition. The vegetable oils that were purchased included canola oil, cottonseed oil, corn oil, sunflower oil, and soybean oil commercially designated as "pure" soybean oil. Quenching performance of these oils was compared to two commercially available quenching oils: Micro Temp 157 a conventional "slow" oil and Micro Temp 153B an accelerated "fast" oil.

Viscosity was measured at 40 and 100°C according to ABNT NBR 10441-10/02. This method is comparable to, the Standard Test Method for Kinematic Viscosity of Transparent and Opaque Liquids and Calculation of Dynamic Viscosity (ASTM D445-06). The time is measured for a fixed volume of liquid to flow under gravity through a glass capillary viscometer at a closely-controlled and known temperature. The kinematic viscosity determined value is the product of the measured flow time and the calibration constant of the viscometer. Two such determinations are needed from which to calculate a kinematic viscosity result that is the average of two acceptable determined values. The range of kinematic viscosities covered by this test method is from 0.2 to 300 000 mm^2s^{-1} at all temperatures.

Cooling curves were obtained under unagitated conditions according ASTM D6200-01, Standard Test Method for Determination of Cooling Characteristics of Quench Oils by Cooling Curve Analysis at bath temperatures of 40, 60, 80, 100, and 120 °C. This test method is based on the 12.5 mm dia. *x* 60 mm cylindrical INCONEL 600. After heating the probe in a furnace to 850 °C, it was then manually and rapidly immersed into 2,000 mL of the oil to be tested, which was contained in a tall-form stainless steel beaker. The probe temperature and cooling times are recorded at selected time intervals to establish a cooling temperature versus time curve.

The accelerated aging equipment used for this work was described previously by Farah (Farah, 2002 and Canale, 2005) which was based on the equipment reported earlier by Bashford and Mills (Bashford, 1984). For this test, a 2.7 L oil sample is placed in a metal beaker which was immersed in a constant temperature water bath where the temperature is cycled between 150 °C and 120 °C every 15 min. The accelerated oxidation was performed under agitation which was provided by using an air flow of 4 L per hour through the vegetable oil being tested. The oxidation test was conducted for 48 h for soybean oil and 60 h for oil palm (since palm oil was found to be significantly more stable) and interrupted every 12 h to determine the fluid viscosity at which time the fluid was returned to the aging system without adding more oil.

Results and Discussion

One of the reactions that occurs when a vegetable oil oxidizes is due to the double bond functionality to react with other double bonds resulting in an overall increase in molecular weight and viscosity (Belinato, 2011). Therefore, one method of monitoring oxidation of a vegetable oil is by monitoring the increase in fluid viscosity of the aging fluid. The test was conducted on uninhibited vegetable oils and the viscosity change from the fresh fluid, after 12, 24 36 and 48 hours is tabulated. The test was stopped after 48 hours because of the large viscosity increases obtained for all of the vegetable oils at this time. For reference, the viscosity change of two fully formulated petroleum oil quenchants was also evaluated. However, since essentially no viscosity change was observed, the testing time was extended to 60 hours at which time only minimal viscosity change was observed. These data were plotted and the results are shown in Fig. 1 and Table 1. The relative order of viscosity increase from best (peanut) to worst (corn) is: peanut < sunflower ≈ cottonseed ≈ soybean < coconut < canola < corn oil.

It is well known that petroleum oil based quenchants exhibit pronounced film-boiling and nucleate boiling (Komatsu, 2009). This is a disadvantage when faster high-temperature cooling is necessary, particularly for crack-sensitive, low-hardenability steels. In such cases,

additives are used to decrease the film boiling behavior by accelerating the wetting of the steel after immersion in oil for cooling. However, vegetable oils do not exhibit the same film boiling or nucleate boiling behavior during quenching as shown in Fig. 2. This is because of the very high boiling points exhibited by vegetable oils under atmospheric pressure conditions. Thus, the surface temperature of the steel decreases below the boiling point and cooling is predominantely by convection. The results obtained in this work are consistent with the relatively fast cooling process reported previously for vegetable oils (Souza, 2009 and Komatsu, 2009).

TABLE 1 VISCOSITY CHANGE WITH RESPECT TO TIME FOR A SERIES OF UNINHIBIED VEGETABLE OILS AND TWO FULLY FORMULATED COMMERCIAL PETROLEUM OIL QUENCHANTS

Aging time (hours)	0	12	24	36	48	60
Cottonseed	30.84	45.27	67.05	93.47	114.43	-
Sunflower	31.03	54.44	55.69	74.60	106.99	-
Corn	31.40	46.98	74.69	121.68	163.13	-
Soybean	29.80	41.07	52.76	94.99	119.67	-
Canola	33.45	59.53	-	87.28	144.84	-
Peanut	33.73	57.33	53.86	64.19	78.96	-
Coconut	26.32	29.80	49.20	92.40	124.10	-
Micro Temp 157	29.00	-	-	34.87	-	35.17
Micro Temp 153 B	40.00	-	-	48.51	-	50.58

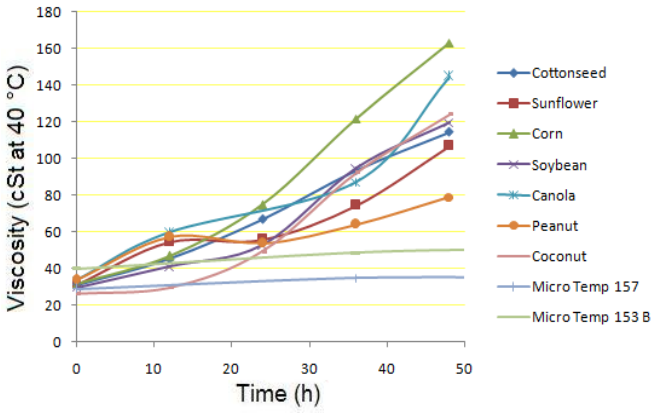

FIG. 1 COMPARISON OF THE VISCOSITY CHANGE WITH RESPECT TO TIME FOR A SERIES OF UNINHIBITED VEGETABL OILS. FOR REFERENCE, THE RESULTS OBTAINED FOR TWO FULLY FORMULATED PETROLEUM OIL QUENCHANTS ARE ALSO SHOWN

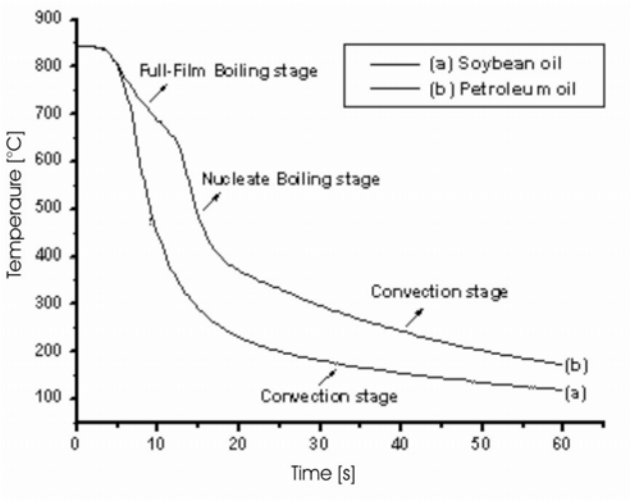

FIG. 2 COMPARATIVE ILLUSTRATION OF THE DIFFERENT COOLING MECHANISMS EXHIBITED BY PETROLEUM OIL AND A VEGETABLE OIL DURING QUENCHING

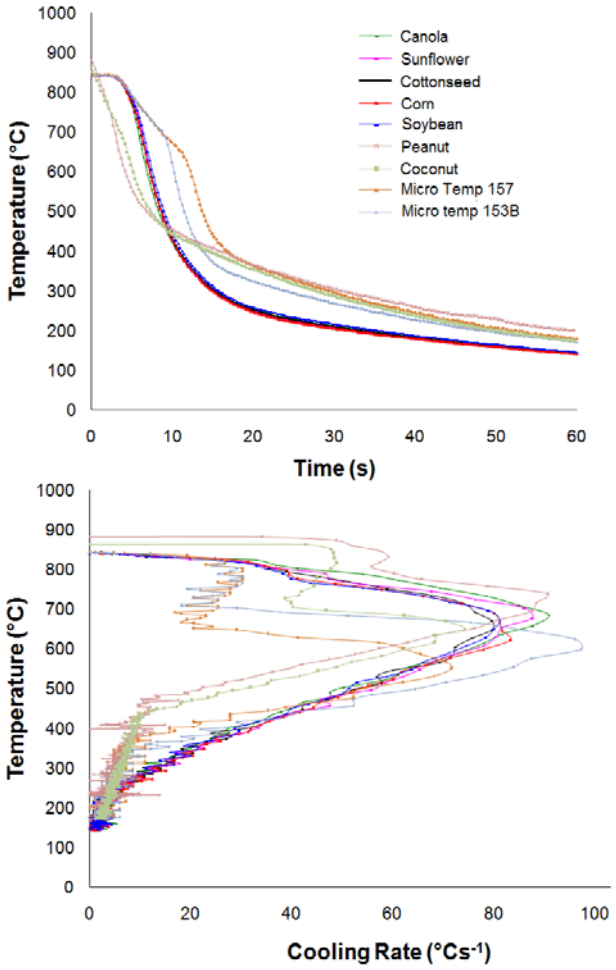

FIG. 3 COOLING TIME-TEMPERATURE AND COOLING RATE BEHAVIOR OF A SERIES OF VEGETABLE OILS AND TWO COMMERCIAL FULLY FORMULATED PETROLEUM OIL QUENCHANT REFERENCE FLUIDS

Most conventional cooling processes involving vaporizable quenchants possess four cooling mechanisms: 1) shock boiling, 2) film boiling, 3) nucleate boiling and 4) convection cooling processes. While shock fim boiling is not observable with the Inconel 600 probe with the thermocouple at the center, the other cooling mechanisms can be seen as shown in Figure 2. Since the ASTM D6200 standard 12.5 mm dia x 60 mm cylindrical Inconel 600 probe provides cooling rate and temperature vs. time at the core of probe, it is only possible to evaluate "average effective heat transfer coefficient (α_{ave})" [16]. During quenching, the value of α_{ave} is dependent on: surface temperature of the steel part (probe), mass and flow of the quenchant at the metal/quenchant (boundary) layer. Since the variation of the heat transfer coefficient during film boiling is typically sufficiently small is is possible to use average values (α_{ave}). During nucleate boiling and convective cooling, average effective heat transfer coefficients can be determined. In this paper, heat transfer coefficients were calculated according to the theory of regular conditions and the calculation procedure described previously by Kobasko, et. al. was used (Kobasko, 2010a and 2010b).

The cooling time-temperature curves and cooling rate curves, of the vegetable oils and of the two petroleum oil quenchant reference fluids, obtained in this work are shown in Fig. 3. With the exception of coconut oil, all of the vegetable oils behaved as depicted in Fig. 2 when compared to the petroleum oil quenchants. However, cooling curve behavior of the coconut oil, which possesses a significantly lower average molecular weight which would correspond to somewhat greater volatility than the other vegetable oils, does exhibit evidence of full-film boiling. The calculated average effective heat transfer coefficients both at 60 and 90 °C bath temperatures are summarized in Table 2.

TABLE 2 AVERAGE EFFECTIVE HEAT TRANSFER COEFFICIENT COMPARISON OF A SERIES OF VEGETABLE OILS WITH TWO COMMERCIAL FULLY FORMULATED PETROLEUM OIL QUENCHANTS

Heat Transfer Coefficient (W/m²K)								
Oil Condition	**New**				**Aged**			
Temperature (°C)	300 – 400		650 – 750		300 – 400		650 – 750	
Bath temperature (°C)	60	90	60	90	60	90	60	90
Cottonseed	319	320	1746	1982	745	1526	2083	1861
Sunflower	660	876	1627	1923	1323	1495	1997	2008
Corn	314	729	1613	1647	1455	1666	1054	943
Soybean	859	469	1630	1973	389	696	1982	2200
Canola	906	472	1560	1936	848	1048	1953	2251
Peanut	312	311	1691	1828	721	1099	1924	2168
Coconut	318	325	947	947	1356	1221	830	1257
Temperature (°C)	450		700		450		700	
Micro Temp 157	1790	-	587	-	-	-	-	-
Micro Temp 153 B	2060	-	705	-	-	-	-	-

The heat transfer coefficient data for fresh vegetable oils in Table 2 shows that all of the vegetable, with the exception of coconut oil, exhibit relatively high heat transfer coefficients in the higher temperature region (650-750 °C) region suggesting that the slow film-boiling process is not occurring. However, coconut oil does exhibit slower cooling in this region suggesting at least incipient film-boiling is occurring. Interestingly, the heat transfer coefficients in the lower temperature region (300-400 °C) are quite variable with no discernable trends. For example, at a 60 °C bath temperature; corn, coconut, cottonseed and peanut oils are substantially slower cooling than canola, sunflower or soybean oil. At the 90 °C bath temperature; coconut, cottonseed and peanut oils are slowest in this region, sunflower and corn oils are fastest with canola and soybean oils being similar to each other and intermediate between the other two groupings. At this time, the reason for this behaviour has not been determined. As expected, the petroleum oils exhibited slow cooling at higher temperature due to full-film boiling and faster cooling at lower temperature with the fast petroleum oil, MicroTemp 153B higher (larger) effective heat transfer coefficients than the slow (or conventional) petroleum oil quenchant, MicroTemp 157.

The effective heat transfer coefficients of the aged vegetable oils is more difficult to analyze. First of all, it is surprising that such a relative small change in heat transfer would result from a large change in fluid viscosity. This indicates that even though vegetable oil quenchant viscosity may increase, the overall heat transfer properties may not exhibit a correspondingly large change. The variability in the two temperature regions, (650-750 °C) and (300-400 °C) mostly follow the same trends observed 1) for the fresh, unaged oils with faster cooling in the high-temperature region and 2) slower cooling in the lower temperature region with coconut oil being the exception although the cooling rate differences between the two temperature regions is considerably closer in most cases than that observed for the unaged vegetable oils.

Conclusions

The oxidative stability of a series of vegetable oils was determined experimentally. Accordingly, the relative order of viscosity increase from best (peanut) to worst (corn) is: peanut < sunflower ≈ cottonseed ≈ soybean < coconut < canola < corn oil. These data show that at least in this test, the peanut oil was the most promising from the standpoint of oxidative stability. However, not surprisingly, the oxidative stability of none of these vegetable oils even closely rivaled the petroleum oil quenchants evaluated as reference fluids. Clearly, the addition of effective antioxidants is required. This work is in progress.

As with other quenching studies reported so far, with the exception of coconut oil, none of the other vegetable oils exhibited film boiling or nucleate boiling. Coconut oil, the vegetable oil evaluated with the lowest average molecular weight, and presumably greatest volatility, did appear to exhibit some full-film boiling behavior typical of what is observed for petroleum oils. These cooling behaviors were verified from the cooling curves and calculated average effective heat transfer coefficients.

Surprisingly, the significant increases in fluid viscosity obtained by ageing, were not reflected in substantial changes in heat transfer.

Research continues into the cooling mechanisms and effect of structure/performance on quenching behavior of vegetable oil both in their native state and after chemical modification. In addition, antioxidant studies are in progress and those results will be reported elsewhere.

ACKNOWLEDGEMENTS

The authors gratefully acknowledge CAPES - Coordenação de Aperfeiçoamento de Pessoal de Nível Superior) and Universidade de São Paulo (USP) for their continued support.

REFERENCES

ABNT NBR 10441-10/02, 2002, "Produtos de Petróleo— Líquidos Transparentes e Opacos - Determinação da Viscosidade Cinemática e Cálculo da Viscosidade Dinâmica," Petroleum Products - Transparent and Opaque Liquids -Determination of Kinematic Viscosity and Calculation of Dynamic Viscosity, Associação Brasileira de Normas Tecnicas ABNT.

ASTM D445-11a "Standard Test Method for Kinematic Viscosity of Transparent and Opaque Liquids (and Calculation of Dynamic Viscosity)", ASTM

International, 100 Barr Harbor Drive, West Conshohocken, PA 19428-2959 USA.

ASTM D6200-01(2007) "Standard Test Method for Determination of Cooling Characteristics of Quench Oils by Cooling Curve Analysis", ASTM International, 100 Barr Harbor Drive, West Conshohocken, PA 19428-2959 USA.

Bashford, A. and Mills, A. J. "The development of improved additives for quenching oils using laboratory simulations", Heat Treatment of Metals, 1984, Vol. 11, No. 1, 9-14.

Belinato, Gabriela et al., "Effect of Antioxidants on Oxidative Stability and Quenching Performance of Soybean Oil and Palm Oil Quenchants", J. ASTM International, 2011, Vol.8, No.9, JAI Paper ID JAI103376.

Canale, Lauralice C. F. et al., "Oxidation of Vegetable Oils and Its Impact on Quenching Performance," Int. J. Mater. Prod. Technol., Vol. 24, No. 1–4, 2005, p. 101–125.

Erdman, K. D. et al., "High-performance biodegradable fluid requirements for mobile hydraulic systems", USA: SAE, 1998, Technical Paper Series, Paper No. 981518.

Farah, Alessandro F. "Caracterização de óleos vegetais como alternativa para meios de resfriamento utilizados no tratamento térmico de têmpera", Dissertação (Doutorado em Ciência e Engenharia de Materiais) – Escola de Engenharia de São Carlos, Instituto de Física de São Carlos, Instituto de Química de São Carlos, Universidade de São Paulo, São Carlos, 2002.

Henry, J. A. "Composition and toxicity of petroleum products and their additives", Human and Experimental Toxicology, 1998, Vol. 17, No. 2, 111-123.

Jones, N. "Managing used oil", Lubes 'n' Greases, 1996, Vol. 2, No. 6, 20-21.

Kobasko, Nikolai I. et al., "Intensive Quenching Systems: Engineering and Design", 2010a, ASTM International, West Conshohocken, PA. ISBN: 978-0-8031-7019-3

Kobasko, Nikolai I. et al., "Vegetable Oil Quenchants: Calculation and Comparison of the Cooling Properties of a Series of Vegetable Oils", Strojniški vestnik (Journal of Mechanical Engineering – Slovenia), 2010b, Vol. 56, No. 2, 131-142.

Komatsu, Daniel et al., "Effect of Corrosion Inhibitors on Cooling Curve Behavior of Soybean Oil-Based Quenchants", Conf. Proceed. New Challenges in Heat Treating and Surface Engineering – Conference in Honor of Božidar Lišcić, June 9-12, 2009, Cavtat Croatia, Publ. by Croatian Society for Heat Treatment and Surface Engineering, Zagreb, Croatia, 37-44.

Otero, Rosa L. S. et al., "Use of Vegetable Oils and Animal Oils as Steel Quenchants: A Historical Review – 1850-2010, Journal of ASTM International, 2011, Vol. 9, No.1, Paper ID JAI103534.

Souza, Ester C. et al., "Comparison of Structure and Quenching Performance of Vegetable Oils", J. ASTM International, 2009, Vol. 6, No. 9, Paper Number JAI 102188.

Souza, Ester C. et al., "Thermal Oxidative Stability of Vegetable Oils as Metal Heat Treatment Quenchants", J. ASTM International, 2011, Vol. 9, No. 1, Paper Number JAI 103817.

Tan, C. P. et al., "Comparative studies of oxidative stability of edible oils by differential scanning calorimetry and oxidative stability index methods", Food Chemistry 2002, Vol. 76, 385–389.

Ester C. Souza is a doctoral student in Science and Materials Engineering at the University of São Paulo (Brazil).

Ms. Ester received her MS in Science and Materials Engineering of the University of São Paulo, and his undergraduate degree in Physics from the Federal University of Ouro Preto (Brazil).

George E. Totten received his BS and MS degrees from Fairleigh Dickinson University in New Jersey and his Ph.D. from New York University in the USA.

Dr. Totten is past-president of the International Federation for Heat Treating and Surface Engineering (IFHTSE) and a fellow of ASM International, SAE International, IFHTSE, ASTM International, IFHTSE and he is a founding Founding Fellow of AMME (World Academy of Materials Manufacturing Engineering).

Dr. Totten is a Research Professor at Portland State University, Portland, OR, an Adjunct Professor in the Department of Mechanical Engineering at Texas A&M University in College Station, TX, and a visiting professor at the University of São Paulo in São Carlos, Brazil.. He is also president of G.E. Totten & Associates LLC, a research and consulting firm specializing in Thermal Processing and Industrial Lubrication problems. Dr. Totten is the author or coauthor (editor) of approximately 600 publications including patents, technical papers, chapters and books.

Lauralice C. F. Canale is an associate professor at the University of São Paulo (Brazil) where she is responsible for Heat Treatment, Tribology and Science and Materials Engineering courses.

Prof. Canale received her MS degree and PhD degrees in mechanical engineering from the same university and conducted Post Doctoral research at the University of Tennessee (USA).

Prof. Canale is a co-editor of 3 books: Failure Analysis of Heat Treated Steel Components (ASM), Theory and Technology of Quenching. 2nd edition (CRC) and a commemorative book "15 Anos do Programa de Post-Graduação em Ciência e Engenharia de Materiais" (EESC/USP). She is an author or co-author of 9 chapters (ASM and CRC books) and over 140 technical papers. She has received various awards and citations and recently received the Fellow of IFHTSE award.

Formation Damage due to Mass Transfer in the Layers under a Dynamic Impact

Victor Zamakhaev[*1]

Geophysical Information Systems Department, Gubkin Russian State University of Oil and Gas

65, Leninsky prospect, Moscow, Russian Federation

[*1]zamvs@mail.ru

Abstract

Studies have shown that the same mechanism is responsible for the accumulation of huge energy in reservoirs and inability to obtain inflow from potentially productive layer. Considering the process of chemical adsorption in layers, it managed to show that when the fluid flows into the reservoir, even moderate magnitudes of over balance internal electromagnetic radiation occur. Under the influence of this radiation, certain order of direction and intensity oscillations of phonons is set. Regard to borehole maximum intensity, oscillations of phonons will take place in the zone of high tangential stresses. Therefore, at some depth from the borehole, wall rock will be destroyed into particles commensurable with clay. Behind the transition layer due to throw of electromagnetic energy into the reservoir and fluid, mass transfer from the periphery of the reservoir to an extended zone with stepwise increased porosity and high thermodynamic compressibility of fluid is formed. Inside this zone a strong and long-range interaction between particles of fluid is developing. Throw in of electromagnetic energy is a result of intensive electromagnetic radiation due to the inflow into the reservoir mud or kill fluid. This formation is called the associate. The associate emits electromagnetic waves that change over allogenic particles in porous medium beyond the associate in the excited state. Between associate and excited particle strong interaction set in, which manifested in attraction of particle to the associate, and it becomes a full member of the associate. Thus, there is a selective implication of allogenic fluid particles into the associate.

Keywords

Chemical Adsorption; Electromagnetic Radiation; Phonon Oscillations; Thermodynamic Coefficient of Extensibility; Accumulated Energy; Rock Pressure; Explosion

Introduction

In many cases, a dynamic impact on the layers is accompanied by mass transfer of reservoir fluids such a water, oil or gas. The dynamic impact on the stratum starts with the first meters of drilling and lasts throughout "life" of wells. Formation exposing with firing guns, increasing the density of perforations, expansion the filter zone, or connection previously nonperforated objects to the working intervals - all these actions are associated with short term intensive impulsive stresses on layers. That all kinds of intensification works of injectivity of injectors and productivity of producers using pulsed - wave technologies should be added.

Mass transfer in the reservoir can be initiated by seismic load of drilling process and start long before entry of drilling tool into this layer. Subsequently recorded during the opening-up of reservoirs water-oil and gas shows or lost returns connect with local natural areas of abnormally high (AHRP) or abnormally low reservoir pressure (ALRP). Without denying existence of such anomalies in nature is still possible to say that in majority of cases petroleum experts deal with the layers which have undergone technological transformations based on mass transfer of reservoir fluid from the periphery to the well or in the opposite direction as a result of seismic load initiated by drilling.

Field case study

From the experience of drilling first exploratory wells both in large and relatively small oil and gas fields, it follows that the mass transfer to the well caused by the drilling accompanied by the occurrence in the vicinity of borehole tremendous energy reserve. This energy can be enough for blow up most of the drill string. Not always energy accumulated in the reservoir is released during drilling, but it can be released when perforation carried out after landing and cementing casing string accompanied kill mud discharge and transition to the unauthorized blowout as it happened on the Bulamar gas-condensate field (Azerbaijan), a number of prospecting and exploration wells of Hapchagaysky megalithic bank and other regions of the Russian Federation. If the supply of energy in the vicinity of borehole is not so great after short term

open hole formation test, it can create the illusion of finding a large deposit of hydrocarbons.

Another extreme reaction to the seismic load during drilling is leaving formation fluid from the borehole wall into the interior of the reservoir. When drilling in mid-and low-permeability reservoir formation, fluid can move away from the well for tens of meters. The process cannot be explained by a simple mud filtrate-reservoir fluid displacement and requires detailed investigation.

Both accumulation of energy in the wellbore zone and withdrawal reservoir fluid from the borehole wall complicate or even make it impossible to obtain inflow from the reservoir.

Table 1 summarizes the results of perforation and cased hole formation tests on the exploration areas of the Hapchagaysky megalithic bank (northeastern Siberia). In the course of drilling wells and selective open hole formation tests, following information about formations was obtained: character of saturation and potential productivity. Bearing capacity of the reservoir rock depending on the effective pressure (difference between rock and reservoir pressure) and character of saturation has not been established. Formation tests after the completion of wells and opening-up with cumulative perforators did not provide hydrodynamic connectivity between downhole and reservoir. Additional mud-acid treatments were ineffective.

Upon the recommendation of the author of this article cased hole formation tests have been repeated after a sufficiently long period of passive idleness. The idea was implemented on the exploratory wells in which potentially productive layers were characterized by unclear character of saturation and sharp decrease in temperature after drilling. For integrity of the experiment, the same schedule-size of the cumulative perforator was used. During the experimental-industrial works, particular attention was paid to the presence at least a weak hydrodynamic connection between gas reservoir and well after the first stage of perforation. Because of presence such connection wellhead pressure could increase as a result of gravitational displacement liquid to gas. However, during the whole period of observation, the appearance of gas at the wellhead was not observed. The following conclusions could be drawn. Firstly, violation by drilling the steady metastable state in the formation has led to behaviour in the reservoir complicated process, which resulted in the layer, got entirely new physical and mechanical properties. Secondly, cumulative perforator shot into the formation with altered physical and mechanical properties is not able to create channels having even low-bandwidth under the action of rock pressure. Thirdly, temperature of the reservoir is reduced and the diffusion of gas to the borehole wall increases supporting strength of the reservoir. In this case, reperforation made in a completely different reservoir properties and new perforation channels provide a hydrodynamic connection between well and layer.

TABLE 1 INFLUENCE ON THE EFFICIENCY OF PERFORATION PASSIVE IDLENESS DURATION OF THE WELLS

Region; Well	**Interval, m**	**Test Result**	**Passive Idleness Duration, Months**	**Choke Diameter, mm**	**Test Result After Passive Idleness Duration, 10^3 m^3/d**
Middle Tyung; 231	3424,8 – 3439,1	no inflow	2	12 mm	80
Peleduyskaya; 751	1549,0 – 1557,0	no inflow	12	10 mm	120
Hotogo-Murbayskaya; 730	2016,4 – 2021,6	no inflow	5	10 mm	135
Mid-Botuobinskaya; 403	1897,6 – 1900,0	no inflow	5	10 mm	120

Theoretical foundations

Despite of particular importance on the consequences of fluids mass transfer for efficiency and environmental safety of prospecting and exploration hydrocarbons, up to the present time, there are no theoretical foundations of mass transfer in the layers under a dynamic impact.

Mass transfer of the fluid in porous media can be considered only in conjunction with the processes in the minerals and their physical properties. Contact of any fluid with the surface of minerals is accompanied by adsorption. There are two types of adsorption: physical and chemical. The distinction between physical and chemical adsorption consists primarily in difference of the forces that hold adsorbed molecule on a solid surface. Forces of electrostatic origin such as the Van der Waals forces, electrostatic polarization

forces and electrical image forces are responsible for physical adsorption. If acting forces are of chemical nature (exchange forces) then such adsorption is called chemical. In this case, adsorption is a chemical compound of the fluid molecule with the solid. Binding energy of the adsorbed fluid molecule with the solid surface in case of physical adsorption is 0.01 eV and only in rare cases can reach 0.1 eV.

Binding energy of chemical adsorption can reach and even exceed 1 eV. Certainly it is not only the difference in magnitudes of the binding energy, but also a fundamental difference between the approaches to consider the interaction of adsorbed molecules with the solid surface and among themselves.

In the case of physical adsorption, system of adsorbed particles fairly interpreted as a two-dimensional gas covering a solid surface. Influence of the adsorbent on the adsorbate is considered as a weak disturbance. Therefore do not expect significant changes in the interaction between adsorbent and adsorbate in case of shear under the action of the pressure gradient.

Situation is different for the chemical adsorption. In this case the adsorbed particles and lattice of adsorbent form a single quantum mechanical system. At the same time, the chemisorbed particles become active participants in the electronic sector of the lattice. In these conditions, the chemisorbed particles are limited in its motion because when moving along the surface, they can to overcome only those energy barriers that do not exceed the binding energy of the particle with lattice of the adsorbent. Large defects and grain boundaries turn out an insurmountable obstacle for them. Shear chemisorbed layer of particles on such defects under an external pressure gradient will break of chemical bonds. The more chemisorbed particles involve in the movement, the greater number of simultaneous breaks of bonds occur. Actually this makes fluid filtration processes close to rocks destruction processes. But the destruction of rocks is associated with electromagnetic radiation, which is recorded through the presence of "windows" in the thickness of the rocks [1]. Under the "window", it should be understood that the area of the reservoir in which electromagnetic waves propagate with very low attenuation.

Based on this, it can be argued that the filtration of fluids in reservoirs characterized by chemisorption will be accompanied by internal electromagnetic radiation, just as it occurs in the destruction of the rocks. This electromagnetic radiation from individual acts of breaking the chemical bonds will not represent interest before the moment of coordination all electromagnetic fluctuations in the area of the current drainage and forming a "window" that extends along the zone of filtration and several orders of greater magnitude than the size of this zone. The chemisorbed particles which gain preferential thermal phase oscillations coinciding with the direction of filtration will also take part in forming a "window". At relatively weak interaction between individual particles of filterable fluid and limited filtration rates, which corresponds to a low-intensity radiation, the effect of fluid ultramobility can be obtained. In case of liquidation external pressure gradient, fluid filtration will continue until the dissolution of ordered thermal oscillations of the fluid particles. Duration of such inertial effect can last for many hours. Sufficiently high intensity of radiation (high filtration rates) will lead to increase in the interaction between particles and enhance fluid compressibility. Final result of the process can turn out to be obliteration [4,5] and disappearance of fluid ultramobility with the impossibility of repetition.

Furthermore, the reaction of minerals to electromagnetic radiation accompanying the filtration of fluids is considered. From the position of quantum theory, any load on a mineral should be compensated by pulses of phonons (associated lattice oscillations). Electromagnetic radiation can provide in-phase coupled oscillations of the lattice within a single mineral, and contribute to the intensity those oscillations which are directed along the lines of maximum stress. Considering the process of chemical adsorption in layers, it managed to show that when the fluid flows into the reservoir, even for moderate magnitudes of over balance $\left(\Delta P_R \geq 2MPa\right)$, electromagnetic radiation occurs (which is not contrary to the fundamental law of electrodynamics: accelerated motion of charged particle generates electromagnetic radiation). This refers to the internal radiation because it occurs inside the porous medium. Under the influence of this radiation, a certain order of direction and intensity oscillations of phonons are set (associated lattice oscillations in quantum representation), corresponding to reduction of external forces acting on the rock minerals. Regard to borehole maximum intensity, oscillations of phonons will take place in the zone of high tangential stresses, i.e. directly in the layers adjacent to the borehole wall.

Experimental procedure

To verify theoretical provisions, high-pressure system has been designed and constructed by the author, in which artificial and natural cores samples length of 150-200 mm and 90 mm in diameter can be loaded by axial and lateral pressures in a special core holder [2] up to a magnitude 80 - 100 MPa. In turn core holder with sample was placed in high pressure vessel. After the creation of loads on the core sample and increasing the pressure in the high pressure vessel (HPV) and in pore volume, initial filtration characteristics of the sample for nitrogen and kerosene were evaluated. Scheme of setup is given in Fig. 1. Core samples of natural rocks mentioned dimensions were drilled out from Grozny outcrops of oil-and gas-saturated sandstones. A number of investigations have been conducted using cores sampled from the Neocomian and Jurassic sediments of Western Siberia, represented by sandstones with clayey and carbonate cement. Artificial core samples were a mixture of certain fraction quartz sand with a marshallitom and liquid glass, compacted in a specific demountable forms and burnt gradually at temperatures of 300 ^{0}C, 500 ^{0}C, 800 ^{0}C and 850 ^{0}C. After final baking from the core faces to eliminate end effects slices length of 20 mm were cut. To compare the effect of different loads on the rock face of core sample directed to the vessel could be opened up to 85 percent or closed with steel disc having a hole along the axis of sample in diameter of 8-9 mm. The last case in the core drilled a hole with the same diameter and length of 70-90 mm. Scheme of sample preparation for installation it into the core holder is given in Fig. 2. To study the influence of rock properties on following effects of the fluid inflow into the formation through the flat face and the cylindrical wall of the channel, artificial core samples were used. These core samples were indicated emission of electrons (the luminescence) during multiple impacts of the indenter (samples of group A) and samples of group B are practically characterized by the lack of emissions [3]. For obtaining comparable conditions of dynamic loads on the layers during drilling and laboratory, studies in high pressure vessel were provided for demolition of small explosive charge.

All studied core samples before installing them into core holder were fully saturated 5-percent aqueous solution of NaCl. Further following operations were performed:

Step 1:

Installing the core in the core holder.

Step 2:

Explosive charge (1.5 g) attached to a breech-block of HPV within 25 - 30 cm from the face of the core was placed above the core holder.

Step 3:

Core holder with an explosive charge went down in HPV and the breech-block was closed.

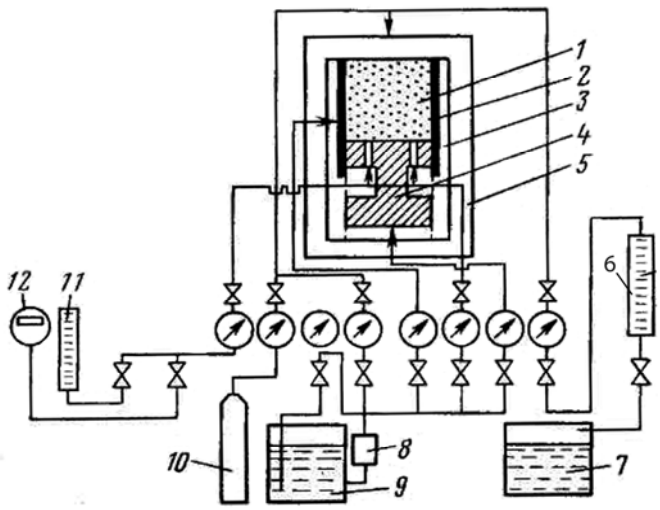

FIG. 1 THE SCHEME OF LABORATORY SETUP

1 — rock sample (core), 2 — rubber sleeve with a metal clip for the lateral hydraulic compression, 3 — casing of core holder, 4 — plunger for axial hydraulic compression and fluid filtration through it, 5 — high pressure vessel, 6,11 — metering tanks, 7 — dump tank, 8 — high pressure hydropump, 9 — initial tank, 10 — gas vessel, 12 — gas meter.

Step 4:

HPV was filled with kerosene and partial displacement of water from the core with kerosene fixing the magnitude of the residual water was carried out.

Step 5:

Kerosene in HPV was replaced by clay mud and then face of core sample or the surface of drilled channel contacted with drilling mud.

Step 6:

The required over balance on saturated core ΔP_R was created simultaneously increased pressure in the drilling mud and in pore volume of the core. The magnitude of over balance varied in the range from 0 to 10-15 MPa.

Step 7:

After maintaining a constant over balance within an hour drilling mud was removed from HPV.

Step 8:

In the process of creating a drawdown ΔP_D during filtration of kerosene through the core the indicator diagram was recorded.

Step 9:

After fillup HPV with drilling mud and creating required magnitude of over balance demolition of explosive charge was carried out.

Step 10:

The drilling fluid was removed from HPV and drawdown was created.

Step 11:

During filtration of kerosene through the core sample the indicator diagram was recorded.

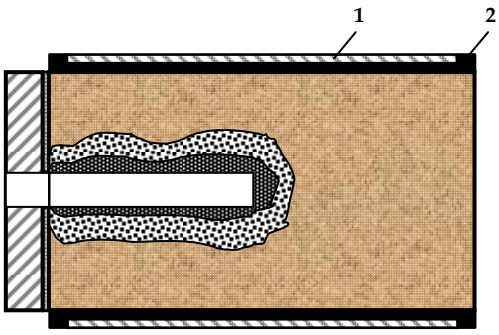

FIG. 2 THE SCHEME OF CORES GROUP A AND B WITH THE CHANNEL AND RUBBER SLEEVE WITH A METAL CLIP. IT IS SHOWN DESTRUCTION ZONE OF THE CHANNEL IN THE SAMPLE OF GROUP A

1- metal clip; 2 – rubber sleeve

The samples of group B did not change its permeability neither under long-term static clogging nor clogging combined with the explosive impact. On flat core, faces of the group B destruction of minerals weren't detected even at $(\Delta P_R \geq 15MPa)$ and mass of the explosive charge 30 g. The results did not change when using core samples of group B with drilled channel and mass of explosive charge increased up to 30 g and the magnitude of over balance up to 15 MPa. Permeability and productivity index of channel managed to restore with reverse kerosene flow in terms of minimal drawdown. On flat core faces of the group A individual minerals of subsurface zone were subjected to destruction, regardless of the mass of explosive charges at overbalance $(\Delta P_R \geq 2MPa)$. Zone of destruction and increased porosity in samples of the group A with a drilled channel at $(\Delta P_R \geq 2MPa)$ are shown in Fig. 2. Using samples of group A with drilled channel showed that combination of clogging at magnitude of over balance $(\Delta P_R \geq 2MPa)$ with explosive impact was accompanied by a sharp decrease in productivity of the channel. Filtration when creating a reverse flow could be carried out only through the bottom of the drilled channel. Investigations after sealing bottom of the channel showed it. Fig. 3 shows the dependence on the magnitude of drawdown ΔP_d kerosene flow rate Q through the bottom of drilled core in the sample of group A and use for clogging with an explosion different liquids and suspensions. Filtration through the lateral surface of the channel was completely absent even at very high drawdown.

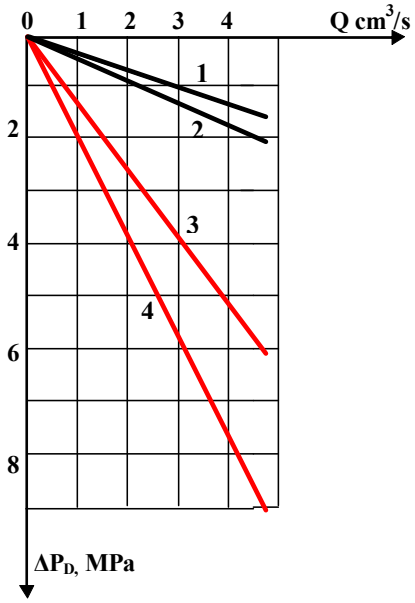

FIG.3 DEPENDENCE ON THE MAGNITUDE OF DRAWDOWN ΔP_D KEROSENE FLOW RATE Q THROUGH THE BOTTOM OF DRILLED CORE IN THE SAMPLE OF GROUP A. MINIMAL STATIC OF OVER BALANCE WAS 2 MPA

The composition of drilling mud:

1 - technical water; 2 - clay solution of 5% NaCl, 5% $CaCl_2$, 5% sulphite waste liquor (SWL); 3 - clay solution of 5% NaCl, 0,5% $CaCl_2$, 5% SWL; 4 - clay solution of 5% NaCl, 5% SWL

Analyzing the experimental results, it can be argued that around the channel at clogging, combined with explosive impact, there has been thrown into a porous medium energy in the form of electromagnetic radiation. In porous medium this radiation with multiple reemissions will persist long enough. In the presence of any recharge emitters with the same frequency, characteristics forming zone will not decay, but can also grow. New formation can be called the associate. Confirmation of the associate occurrence

and its properties is the strong magnetization of a metal clip, placing outside of rubber sleeve in core holder (Fig.2). Despite having made a complete demagnetization of clip before clogging with the explosion, it again is magnetized. Magnetization of clip is completely absent when using during explosive clogging samples of group B. Detailed investigations have shown that when trying to create in the associate gradient of pressure by external pressure, counterpressure on its boundary occurs. This counterpressure is equal to the magnitude of external pressure and focused in opposite direction. Thus, directed thermal oscillations of the particles in fluid create on the boundary impassable obstacles for penetration of external pressure into associate. In fact, the emergence of counterpressure at the associate boundary is similar to appearance of counterpressure at the boundary of the mineral loaded under any direction at the expense of codirectional oscillation of phonons. Therefore to displace water with kerosene from the zone around the channel was not possible both when creation of high drawdown and significant increase of pore pressure in the core.

The change of core's volume is investigated. To study the maximum strain core samples of the group A in radial direction at clogging with explosive impact, thin copper wire in a few turns was wound on the sample and the ends of wire were soldered. Fig. 4 shows the scheme of core with winded wire to determine

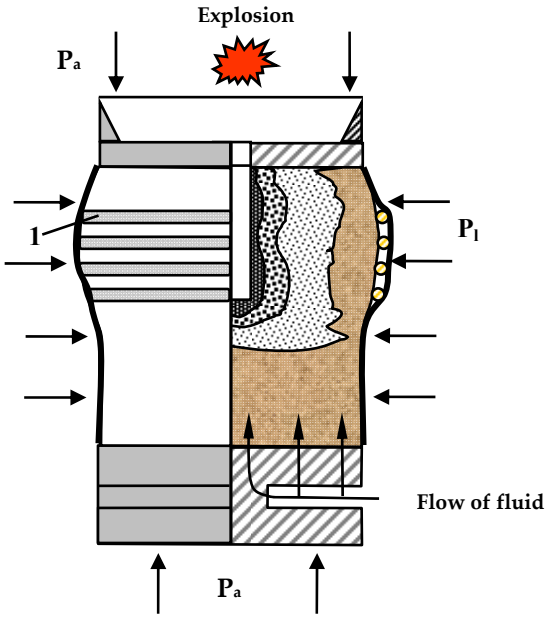

FIG. 4 CORE WITH WINDING OF THIN WIRE

P_a – axial pressure; P_l – lateral pressure;

1 – winding of wire

maximum radial strain. Knowing the initial and final length of the wire after the deformation associated with explosive clogging, it is easy to determine the maximum value of radial strain. In the experiments this value was about of 2 absolute percent at residual water saturation of 10%. Virtually all of the residual water moved into the zone of phase transition.

With the growth of core water saturation, maximum radial deformation of the sample also increased. So after the explosive impact at 30-40% of water saturation, maximum radial strain was 6 and more absolute percent, but the upper part of the core was completely destroyed in spite of very high value of hydraulic compression (50 - 80 MPa). Scheme of core destroying is given in Fig. 5.

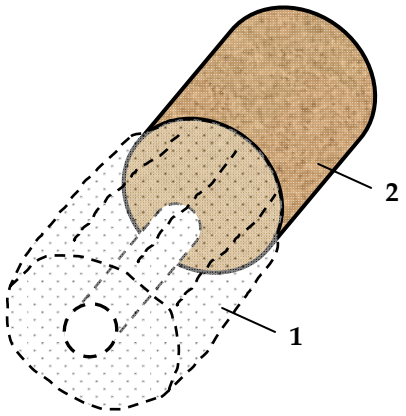

FIG. 5 DESTRUCTION OF CORE AROUND THE CHANNEL

1 – destroyed part of core; 2 – undamaged part of core

Using samples of group A, mass transfer in the core after the creation of associate was studied. For this purpose, evaluation of fluid mass transfer after the increase of pore volume in core samples of the group A was carried out in the following way. Upon completion of cake formation on the surface of drilled channel from the CMC-treated (1.5%) mud and creation of over balance magnitude 2 – 3 MPa, an explosive impact on the sample within the HPV was carried out. Moving in the core of water containing colloidal particles of SiO_2 was monitored using the Mariotte vessel located outside of HPV. The residual water saturation of the core was not more than 10% (taking into account the mud filtrate). Pipeline from the core holder was connected to the Mariotte vessel filled with tinted liquid to a level 0-0. Decrease or increase level of liquid in a transparent capillary after the explosion provided an indication of the direction fluid movement in the core. The scheme of the test bench is shown in Fig. 6. In samples of group A, liquid moves to the explosion despite a sufficiently large

magnitude of over balance $\left(\Delta P_R \geq 2MPa\right)$ (Fig. 7). Air breaks through the bottom end of the capillary below the point L. One of the reasons of fluid movement to the explosion consists in increasing porosity of the sample during the formation of associate. However, the additional pore volume would be filled in a few seconds. At the same time the movement of fluid towards the explosion in the core continued for tens of minutes, which indicates that the volume of fluid in the core went to decrease and to complete the process required a lot of time (tens of minutes). By additional studies after extraction of core from laboratory setup, the absence of water in the core was detected.

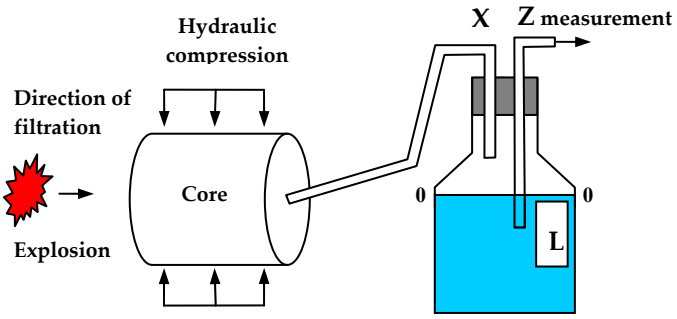

FIG. 6 SCHEME OF SETUP FOR DETECTION OF SMALL FLUID DISPLACEMENTS IN THE CORE. POINT L – THE LOWER LEVEL OF THE CAPILLARY Z

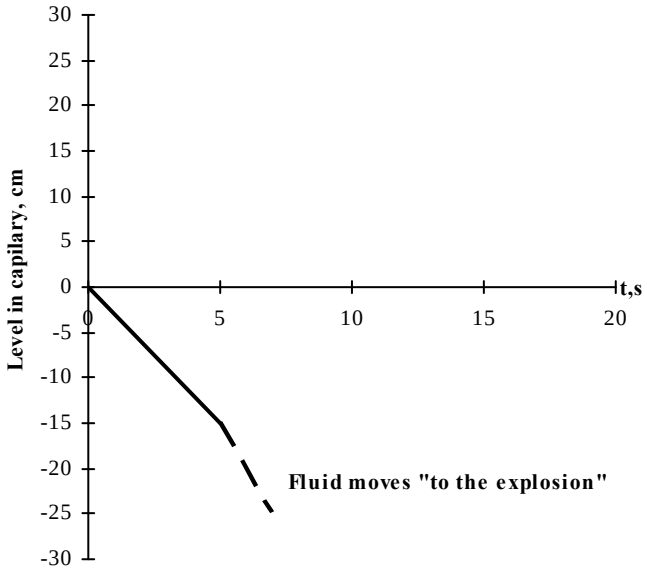

FIG. 7 DYNAMICS OF LIQUID LEVEL IN CAPILLARY AFTER THE EXPLOSION. SAMPLES OF GROUP A

Making use of scheme shown in Fig. 8. Appearance of associate led to an increase of porosity and compressibility of aqueous colloid. Mixture of kerosene and water, remaining outside the associate, will be subjected to electromagnetic radiation by association in which between particles of the fluid, located in the energetically excited state, there are tremendous forces of gravity. Particles of aqueous colloid, located outside the associate, but in a porous medium, when excited by electromagnetic radiation of associate under the action of gravity, move towards the associate (Fig. 8a). This movement takes place with acceleration due to increase of the radiation intensity from the movement of the particles themselves. As a result, the particles become full members of the associate, bringing into it an additional electromagnetic radiation.

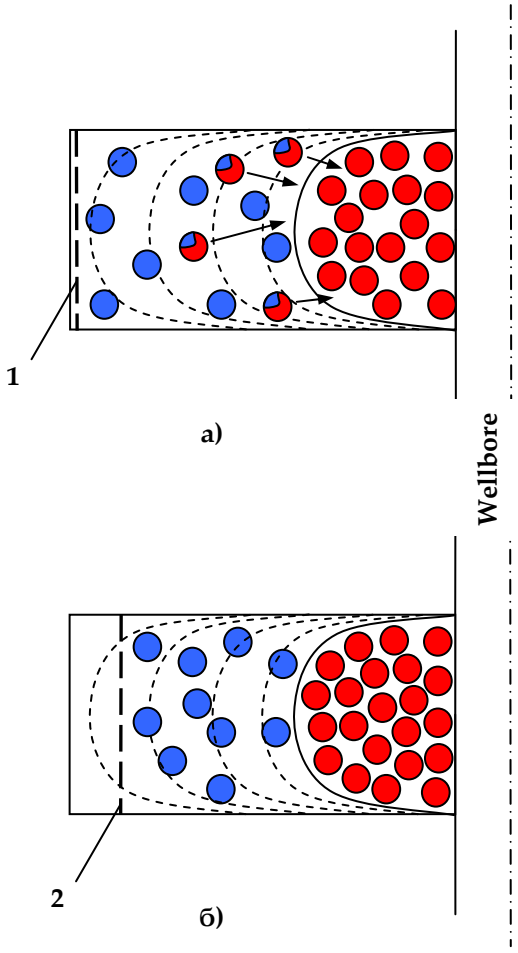

FIG. 8 SCHEME OF IMPLICATION OF EXCITED PARTICLES INTO THE ASSOCIATE: A) THE BEGINNING OF THE PROCESS

B) THE LAST STAGE OF THE PROCESS

- fluid particles in the excited state

- particle of fluid excited by the associate

- electromagnetic radiation

1 - initial boundary of the fluid in the core of the group A

2 - the border after implication of the excited particles into the associate in the core of the group A

Fluid particles of otherwise origin are not excited at frequencies of electromagnetic radiation of the associate, and, being allogenic, don't interact with associate. Therefore all particles of aqueous colloid are implicated in the associate, and after a strong compression their volume decreases that leads to the release of volume in the core. It is schematically shown in Fig. 8b. Moving of fluid particles in the associate occurs quite slowly that was detected during the experiments. Thus, due to selective movement of particles of aqueous colloid into the associate, last-mentioned will increase a volume and store energy.

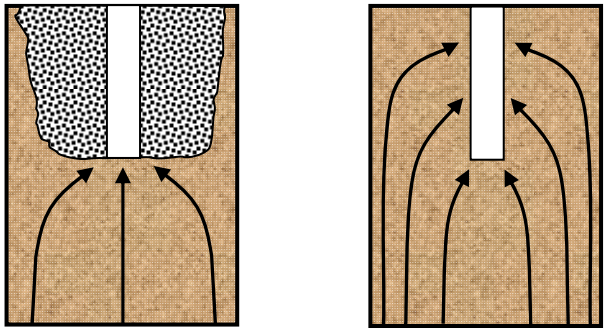

a) b)

FIG. 9 SCHEME OF KEROSENE FILTRATION THROUGH THE SAMPLES OF GROUP A WITH THE CHANNEL AFTER FORMATION OF THE ASSOCIATE AROUND THE CHANNEL (A) AND AFTER A TEMPORARY DISCHARGE CORE FROM THE HYDRAULIC COMPRESSION AND RECOVERY OF HYDRAULIC COMPRESSION (B)

The associate in the core is stored for a long time (for many weeks) without recharging from external emitters, but, it is rapidly destroyed when unloading from the rock pressure (hydraulic compression). Fig. 9 shows the scheme of kerosene filtration after formation of the associate around the channel (Fig. 9a) and after a temporary discharge core from the hydraulic compression and recovery of hydraulic compression (Fig. 9b). Hence emerged metastable state in the reservoir can exist only at presence of rock pressure and, in a great measure, due to rock pressure.

Conclusions

During drilling or killing the well for repair works in a wellbore area of reservoir zones can be formed, where accumulation of energy because throwing into the reservoir electromagnetic energy and fluid mass transfer from the periphery of the reservoir to the wellbore takes place. Throwing into the reservoir of electromagnetic energy is a consequence of mud or kill fluid inflow into the layer at high overbalance. This process can occur only in layers at low electronic work function to the surface of minerals.

Zones with accumulated energy are characterized by strong and distant interaction of particles between themselves and therefore the fluid in these zones has a high thermodynamic compressibility.

The associate is capable of growth and accumulation energy by implication into itself congenerous particles.

The associate is resistant and on the stage of development insensitive to external influences.

Based on laboratory and field studies, it can be argued that the associate can persist for months

During completion of energy accumulation, sensitivity of the associate against external influences sharply increases and even comparatively weak impulsive impact can result in release of enormous energy and the emergence of an ecological catastrophe.

The emergence of associate is impossible without the internal electromagnetic radiation generated by a filtration of fluids.

The associate creates impassable obstacles for fluid filtration and, therefore, complicates the process of prospecting, exploration and development of hydrocarbon deposits.

REFERENCES

Bogdanov, Y. A., and Pavlovich, V. N. "Nonequilibrium radiation of the Earth's crust - an indicator of geodynamic processes", Geophysical Journal, 30 (4), pp. 12-24, 2008.

Gayvoronskiy, I.N., and Zamakhaev, V.S. "Oil and gas reservoirs of Western Siberia. Their penetration and testing", Moscow, ZAO Geoinformmark, 2000.

Zamakhaev, V. S., and Ivanov, A.N. "Core holder for the study of filtration processes in rocks," A.U. Patent 145 6844, 1989

Zamakhaev, V.S., and Kolobov, M.A. "Emission phenomena during mechanical destruction of deep-laying sedimentary rocks". Abstracts of XI All-Union Symposium on Mechanochemistry and Mechanical emission of solids, Moscow , 1990

Zamakhaev, V.S., and Martynov, V.G. "Wellsite explosive operations," Moscow, Nedra, 2010

Victor Zamakhaev earned his PhD degree in the field of physics of reservoir from Moscow Engineering and Physical Institute. For a long time he worked for All-Russian Scientific Research Design Institute of Explosive Geophysics where he was head of well completion and testing department. Also he has taken different position in Gubkin Russian State University of Oil and Gas during the past ten years.

Victor Zamakhaev is the author of many books and articles at the field of petroleum engineering: *Wellsite explosive operations* (Moscow, NEDRA, 2010), *Processes in petroleum reservoirs, initiated by the dynamic stimulation* (Quality Management in oil-and-gas complex, №1, 2011). His research work is directed to processes in petroleum reservoirs under filtration and dynamic stimulation.

Identification of Carbon Dioxide-Producing Microorganisms Originating from Mexican Oil Wells with Potential Application in Oil Recovery

Regina Hernández-Gama*[1], Ana Muñoz-Colunga[2], Emma A. Hernández-Mendoza[1], Luis Torres[3], and Norma G. Rojas-Avelizapa[1]

*[1]Biotecnología, Centro de Investigación en Ciencia Aplicada y Tecnología Avanzada, Cerro Blanco 141, CP 76090, Querétaro, México. [2]Investigación, Instituto Mexicano del Petróleo, Eje Central Lázaro Cárdenas Nte 152, CP 07730, D.F., México. [3]Bioprocesos, Unidad Profesional Interdisciplinaria de Biotecnología, Av. Acueducto s/n Barrio la Laguna, Ticomán, C.P. 07340, D.F., México.

*[1]regina_gama@hotmail.com; [2]mcolunga@imp.mx, [1]nrojasa@ipn.mx

Abstract

The present study examined the growth and the CO_2 production of indigenous microbial cultures collected from three zones in Chicontepec oil reservoir located in Veracruz, Mexico. Two microbial cultures, coded as NW O and CW O, showed an accelerated growth and higher CO_2 production when molasses were used as carbon source. They were selected and identified by molecular-biology techniques as potential candidates to be used in future Microbial Enhanced Oil Recovery studies. To improve CO_2 production, a reformulated culture medium was evaluated using only the culture coded as NW O which showed the better growth. Results showed that the reformulated culture medium caused an increase in the production of CO_2 from 1.64$gL^{-1}$to 3.13 gL^{-1} by the NW O culture. Analysis of 16S rRNA gene libraries allowed the identification of fermentative microorganisms; the NW O culture is composed of *Thermoanaerobacter pseudethanolicus* and *Thermotoga neapolitana*; the CW O culture is composed of *Caldanaerobacter subterraneus*.

Keywords

MEOR; Petroleum Microbiology; CO_2 Production

Introduction

Chicontepec is an area with an important accumulation of hydrocarbons in Mexico (CNH, 2010; Gachuz-Muro and Sellami, 2009; Rafique and Ali, 2008). It was recognized as an important reserve, with a calculated original oil in place of 140,900 million short tons (Gachuz-Muro and Sellami, 2009), and an estimated original volume of 136,784 million barrels and an original gas volume of 54,222 billion cubic feet, but total cumulative production has only reached 160 million barrels of oil and 270 billion cubic feet of gas (CNH, 2010; PEMEX, 2011). The Chicontepec field contain oil from 18° to 45°API, in laminated sandstones with a maximum porosity of 14%, at a depth of around 2500 meters. Oil extraction in Chicontepec is a complex task, due to the heterogeneous distribution of sandy zones, low permeability from 0.01 to 10 mD (milliDarcies) and mixed wettability of the rock, among others (Bermúdez et al., 2006; Gachuz-Muro and Sellami, 2009). Such characteristics make Chicontepec be a reservoir of low recovery and development (CNH, 2010). To facilitate the extraction of oil in a heterogeneous medium of low permeability, it is necessary to increase oil mobility, and technologies with a biological component have interesting potential in this respect.

Microbial techniques known as MEOR (microbial enhanced oil recovery) improve oil recovery through the use of microorganisms and/or their by-products in depleted oil reservoirs (Belyaev et al., 2004; Bryant and Burchfield, 1989; Thomas, 2008). During the last two decades, MEOR testing has been reconsidered in the search for high-performance and cost-effective extractive technologies. The success of MEOR depends strongly on the microbial metabolism, which in turn is determined by the type of microorganisms present in the reservoir. Mechanisms by which bacteria can help recover the trapped oil have been explored, but they are not completely understood since they can be quite complex and may involve multiple biochemical processes (Sen, 2008). Gas production is one of the

possible action mechanisms. The CO_2 produced by the bacteria improves the oil recovery in two ways: by reducing oil viscosity through its diffusion in oil (Enick and Olsen, 2012) or by increasing the pressure inside the reservoir (Donaldson and Clark, 1982).

The main source of the produced gases is *in situ* fermentation of carbon sources, carried out by anaerobic bacteria (Jack, 1982). However, there are doubts about whether CO_2 can be produced microbiologically in sufficient quantities to displace oil trapped in the rock (Rafique and Ali, 2008). The most important and most frequently discussed gas-producing bacteria are *Clostridium*, *Desulfovibrio*, and *Pseudomonas* (Bryant and Burchfield, 1989).

Based on the considerations referred to above, and taking into account the nature of the Chicontepec oil field, the *in situ* production of CO_2 should improve the properties of the rock-fluid system, because CO_2 is highly miscible with oils with densities from super light to medium. CO_2 can reduce the viscosity of the oil and the tension of the oil-water interphase, forming solutions which can tunnel through the rock, increasing its permeability.

In MEOR studies, data about the species that compose microbial consortia in a particular oil deposit are important because they provide an understanding of the ecological functions of microbial groups in that specific environment and their metabolic capabilities. In general, microorganisms have been reported as responsible for the accumulation of metabolic products or by-products that transform the brine chemistry. These changes may modify the hydraulic properties of the rock and the conditions of hydrocarbon migration, suggesting their potential applications for oil extraction (Wolicka et al., 2010).

The purpose of the present study was to evaluate the ability of native microbial cultures from the Chicontepec basin to produce CO_2 and to increase this production by reformulating the culture medium. Also, identification of these microorganisms will suggest options for their use in new applications for oil extraction.

Methodology

Site Description

This study was carried out with samples obtained from the Chicontepec oil reservoir, located in east-central Mexico, covering parts of the states of Veracruz, Puebla, and Hidalgo (CNH, 2010). Geologically it covers an area of 3875 km^2; the formation is located in a great depression and it is formed by sandstone with interbedded shale and silty shales. It is composed of carbonated rocks with sediments highly cemented by ferrous calcite and dolomite (Bermúdez et al., 2006). The temperature of the wells in the reservoir ranges from 70°C to 100°C, with oil quality from light to heavy (CNH, 2010).

Sampling of the Crude Oil

Microorganisms were obtained from samples that came from oil wells in three different zones: north, central and south Chicontepec basin, north well (NW), central well (CW) and south well (SW). Some characteristics of the three samples have been reported elsewhere (Torres et al., 2012). Samples collected from production wellhead, were placed in 19 L polyethylene bottles filled to the top to prevent oxygenation, and transported to the laboratory, and valves were cleaned with solvents and drained. They were stored at room temperature in the dark. The physicochemical characterization of the samples was done according to methods IMP 151803-07 and IMP 151803-14; the results are given in Table 1.

Obtaining Microbial Cultures from Oil Samples

Culture medium. The fermentative microbial cultures were obtained using SI medium containing (in gL^{-1}): NaCl (35), NH_4Cl (0.25), K_2HPO_4 (0.14), KCl (0.33), $CaCl_2{\cdot}2H_2O$ (0.14), $MgCl_2{\cdot}6H_2O$ (1), cysteine-HCl (0.5), resazurine 0.1% (1 mL), yeast extract (2), and casein peptone (2), with cane molasses (10) as carbon and energy source (López-Ramírez, 2005).

TABLE 1 PHYSICO-CHEMICAL CHARACTERISTICS OF OIL SAMPLES FROM CHICONTEPEC

Parameter	North Well (NW)	Central Well (CW)	South Well (SW)
Well Temperature (°C)	70	70	100
Water Content (%)	52.4	3.8	0.2
Salt Content of Dehydrated Oil (gL^{-1})	14.76	16.40	24.60
°API	29.2	21.9	18.7
pH of the Associated Water	8.36	7.90	7.23

Muñoz-Colunga (unpublished data)

Fermentative microbial cultures were obtained directly from the oil samples, or after a centrifugation which separated the oil phase from the brine; these sources were coded as O, OD, and B (for oil, oil

dehydrated, and brine, respectively). A total of nine samples were thus obtained. Of each of these samples, 2 ml were used to inoculate 30 ml of culture medium in a sealed 125 ml serum bottle (Table 2). Cultures were coded using the name of the sample and the corresponding fraction: oil dehydrated (OD), oil (O), or brine (B).

Bottles were incubated for 10 days at 70°C for the NW and CW samples, and at 100°C for the SW sample. Subsequently, observing the microbial culture growth indirectly by the increase in turbidity, fresh cultures were prepared by transferring 2 ml to fresh SI medium. Previous cultures were used in subsequent experiments and to preserve microbial cultures. All procedures were performed under anaerobic conditions, using a N_2 atmosphere.

TABLE 2 SAMPLE CODES ESTABLISHED BY THE PHASE USED AS INOCULUM.

Sample	Phase of Inoculum	Code
NW	Oil	NW O
	Oil Dehydrated	NW OD
	Brine	NW B
CW	Oil	CW O
	Oil Dehydrated	CW OD
	Brine	CW B
SW	Oil	SW O
	Oil Dehydrated	SW OD
	Brine	SW B

Selection of the Best CO_2-producing Cultures

Once the microbial cultures had been obtained, microbial growth was evaluated in SI culture medium for 60 h at 70°C or 100°C, depending on the sample. The parameters evaluated were CO_2 production, total protein, and total sugars. CO_2 was evaluated as the product of the metabolism of interest, and total protein was considered as growth indicator, and sugar consumption as a yield parameter.

The CO_2 production of fermentative bacteria was evaluated removing 1 ml volumes of the head space of the serum bottles using gastight syringes and analysing these samples by gas chromatography through a CTR-1 column fitted with a TCD. Helium was used as the carrier gas, at a flow rate of 65 ml min^{-1}. The temperatures of injection port, oven, and detector were 45°C, 22°C, and 100°C, respectively. The cultures were allowed to cool to room temperature prior to gas sampling. The CO_2 produced was calculated by the ideal-gas equation.

Protein was determined by the Bradford method: 1 ml of biomass was centrifuged at 10,000g for 20 min and suspended in 1 ml saline solution (SS). This solution was again centrifuged; then, the pellet was suspended in 0.25 ml of SS and lysed by adding 0.75 ml of 0.1N NaOH and incubating at 80°C for 1 h. The resulting supernatant was used for the Bradford protein micro assay (Bradford, 1976).

To assess the consumption of the carbon source (molasses), total sugars were quantified by the fenol-sulfuric acid method (DuBois et al., 1956), using a glucose/sucrose curve as standard (0-100 $\mu g\ mL^{-1}$).

Evaluation of CO_2 Production and Microbial Growth by Cultures NW O and CW O

With the microbial cultures showing the highest CO_2 production, two kinetic studies were carried out, using sealed 125 ml serum bottles containing SI culture medium (30 ml), each inoculated with 2 ml of cultures NW Oor CW O. Microbial culture NW O was incubated for 57 h and culture CW O for 100 h, at 70°C. Bottles were sacrificed about every 4 h to analyse total protein, sugar consumption, and CO_2 production.

Effect of Reformulated Medium in the Increment of CO_2 Production

Based on previous results and with the aim to enhance CO_2 production, a reformulated culture medium (coded as SR medium) was used for culture NW O. The SR medium is similar to SI medium, with the following modifications: the molasses concentration was increased from 10 to 17 gL^{-1}, and buffer was added to maintain pH 7 during the whole incubation period. Additionally, the inoculum was increased to 3 ml. The SR medium was tested incubating the culture NW O for 165 h in serum bottles containing 30 ml of culture medium under anaerobic conditions at 70°C. CO_2 production was evaluated chromatographically as described above.

Microbial Identification

Total genomic DNA was extracted from 20 ml of fresh microbial cultures NW O and CW O with the Illustra tissue & cells genomicPrep kit (GE healthcare, USA), following the instructions for tissue extraction. DNA quality was estimated by electrophoresis through a 1% agarose gel in 1X TAE buffer, stained with ethidium bromide (Sambrook and Russell, 2001).

PCR amplifications of the 16S rRNA gen were performed with a Techne TC-3000 Thermal Cycler (Barloworld Scientific, USA), using universal bacterial primers (Relman, 1993). The reactions were done in 50 µl mixtures containing 5 µl of 10X PCR buffer, 0.4µM of each of the primers coded as "8" and "1492"in reference (Relman, 1993), 100µM of each of the four dNTPs, 3 mM $MgCl_2$, and 2U of Taq polymerase (Fermentas). Amplifications were done using an initial denaturation step of 94°C for 5 min, followed by 35 cycles of 1 min at 94°C, 1 min at 55°C, and 1 min at 72°C, and a final extension at 72°C for 5 min. PCR products were checked in 1% agarose gels stained with ethidium bromide solution, and stored at -20°C for subsequent cloning.

Two 16S rRNA gene libraries were constructed by cloning PCR-products, previously purified using the Illustra GFX PCR DNA and gel band purification kit (GE healthcare). The purified PCR fragments were then cloned into pJET 1.2/blunt (Fermentas) by using the CloneJET PCR cloning kit (Fermentas), and the resulting ligation products were used to transform competent *Escherichia coli* JM107 cells (Fermentas) with the TransformeAid Bacterial Transformation Kit (Fermentas). Positive clones were detected as colonies on solid medium containing ampicillin (50 µg ml^{-1}).

Recombinant plasmids were isolated from overnight cultures using the Illustra DNA plasmid spin kit (GE healthcare), and restricted with *Bgl* II (Fermentas) to detect the inserts. Library clones were analysed by RFLP, digesting with *Dde* I and *Hae* III (Invitrogen) and subjected to 3% agarose electrophoresis. The clones were grouped according to their RFLP patterns and one clone for each RFLP pattern was selected for sequencing. Different RFLP patterns with identical sequences were considered as a sole phylotype.

Sequences of 470 to 1,583 nucleotides of each RFLP representative library clones were sequenced using the forward and reverse pJet1.2 sequence primers (Fermentas) at LANGEBIO, CINVESTAV, Mexico. The 26 new sequences reported herein were deposited in the GenBank with the access numbers JF754941-JF754966. The sequences were examined by the CHIMERA-CHECK online analysis program of the Ribosomal Database Project-II and assembled with DNA Baser version 2.11.0.933 (Heracle Software, Germany). The partial sequences were then subjected to a BLAST search version 2.2.3 (Altschul et al., 1990) to explore the taxonomic hierarchy of the sequences. A collection of taxonomically related sequences obtained from the NCBI Taxonomy Homepage was used to perform a multiple alignment analysis with CLUSTAL X (Thompson et al., 1997). Multiple alignments were manually edited using SEAVIEW software (Galtier et al., 1996). Only common 16S rRNA gene regions were included in the phylogenetic tree, and similarity analyses using the Jukes-Cantor and Kimura 2-parameter models were performed with the MEGA version 5 program (Tamura et al., 2011). The phylogenetic trees were constructed using the neighbor-joining method, and 1,000 bootstrap replications were assessed to support internal branches (Hillis and Bull, 1993). The similarity percentages among sequences were calculated using BioEdit 7.0.5.2 software (Hall, 1999). The genus and species limits were 95% and 97%, respectively, according to previously suggested criteria (Rosselló-Mora and Amann, 2001).

Results and Discussion

Obtaining Fermentative Microbial Cultures

Fermentative microbial cultures were obtained from eight of nine oil fractions of three samples. Brine from sample SW contained no cultivable fermentative bacteria. The common microscopic morphology observed in the samples corresponded to Gram-negative, rod-shaped bacteria, but cultures NW O and SW O also contained Gram-negative cocci.

Microbial growth was more evident in oil (O) and brine (B) samples. In the literature, a wide diversity of microbes has been reported in brine samples; the authors explain these findings with the availability of nutrients, salts, and cofactors in brine (Bonch-Osmolovskaya et al., 2003; Dahle et al., 2008). Other authors report that microbes are associated only with oil droplets (Magot et al., 2000). The present study examined microbial cultures from different crude-oil phases, to cover the possible metabolic diversity.

The composition of the culture medium and the conditions of incubation, mainly temperature and salinity, are responsible for the selection of microbes that can tolerate oil-well conditions. This aspect is relevant since some authors have speculated about the origin of the microbes, i.e., if the microbes are indigenous or introduced after well perforation (Dahle et al., 2008). The identification of the microorganisms is useful not only for the application of MEOR technologies, but also for the description on the microbial activity within the reservoir, to understand the possible biodegradation of crude oil, and to describe the *on-site* interaction between different metabolic groups (Head et al., 2003; Town et al., 2009).

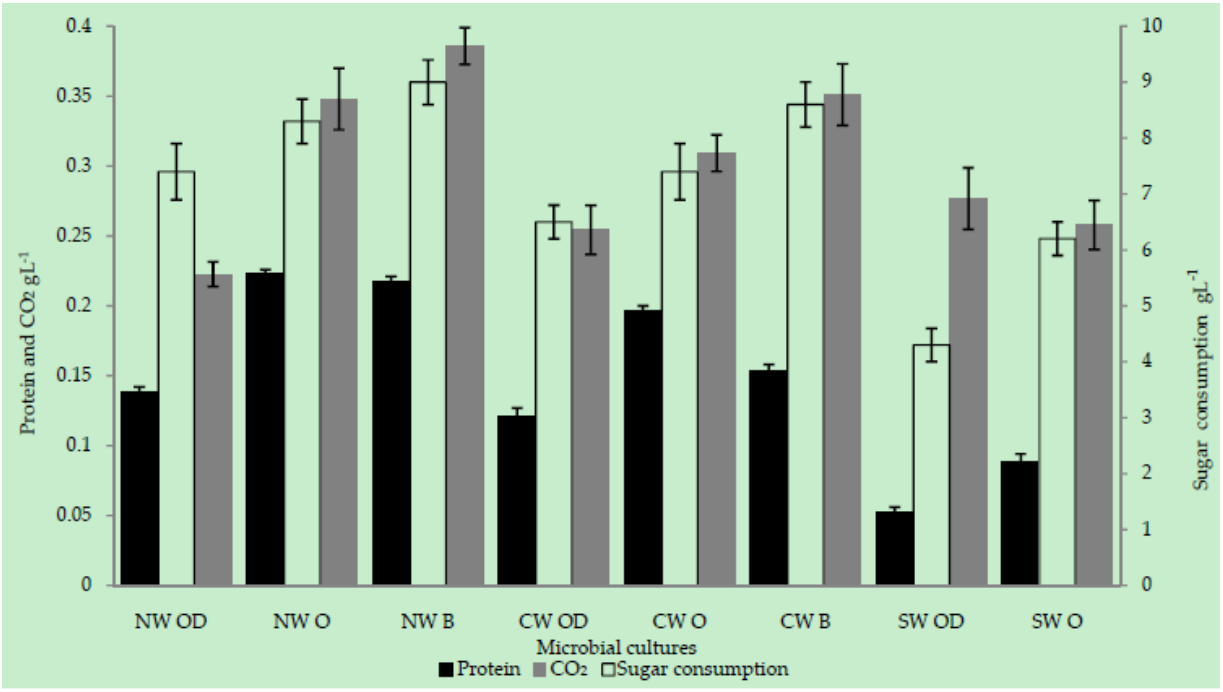

FIG. 1 CARBON DIOXIDE PRODUCTION OF MICROBIAL CULTURES ORIGINATING FROM CHICONTEPEC OIL WELLS. CULTURES WERE INCUBATED FOR 60 H AT 70°C OR 100°C IN SI CULTURE MEDIUM

Fermentative microbes are expected to be useful in MEOR technologies because of their wide distribution in oil reservoirs. Most of them are considered indigenous organisms (Bonch-Osmolovskaya et al., 2003; Dahle et al., 2008; Orphan et al., 2000). Fermentative microbes produce CO_2 and H_2, which are relevant to ecological microbial interactions and also important because of their impact on the composition and properties of the oil (Wolicka et al., 2010).

Selection of CO_2-producing Cultures

To select the microbial cultures with the highest yield, CO_2 production, and growth rate, treatments were evaluated after 60 h of incubation. Criteria for selection were microbial growth measured by turbidity (data not shown) and the highest CO_2 yield using the least amount of sugar.

Fig 1 shows results of experiments after 60 h of incubation. As it can be observed, microbial growth (protein) correlates with biogas production; also, it is seen that microbial cultures SW OD and SW O were those with poor growth and low CO_2 production, possibly due to the fact that the Southern region of the reservoir has the highest temperature, one of the most limiting factor for microbial growth (Stetter and Huber, 1999). Other characteristics of SW (Table 1) that could restrict microbial growth are its low water content (0.2%) and high salt content (24.6 gL^{-1}). Samples from NW and CW had salinities of about 1.4-1.6 gL^{-1} and water content of 52.4% and 3.8%, respectively.

Sugar consumption and biogas production were monitored to evaluate the CO_2 yield in relation to the sugar content. In culture NW O a yield of 41.9 mg CO_2 g^{-1} of sugar was reached after 60 h of incubation, while culture CW O reached 41.8 mg CO_2 g^{-1} of sugar at the same time. Although cultures of NW B and CW B reached a yield of 42.8 mg CO_2 g^{-1} of sugar and 40.8 mg CO_2 g^{-1} of sugar, there is no significant difference in CO_2 yield between cultures from oil and those from brine; therefore, microbial cultures showing rapid growth were selected for the further work.

Evaluation of CO_2 Production and Microbial Growth by NW O and CW O

Once the microbial cultures with the highest production of CO_2 had been selected, kinetic studies were undertaken with them. As it can be observed in Fig. 2, there is a correlation between protein and CO_2 production (Fig. 2A and 2D).

CO_2 production was successful with molasses as carbon and energy source. During microbial growth, the pH decreased from 7 to 5 (Fig 2C and 2F). One of the essential factors determining microbial growth is pH which in oil fields runs from pH 4 to pH 9. Chicontepec samples have pH values between 7.23 and 8.36. Changes in pH observed under laboratory

conditions may not realistically reflect corresponding changes in the oil reservoir; nevertheless, even changes by only one pH unit in an oil well could cause changes in the chemical interactions between rock and brine, affecting oil extraction. Additionally, changes in pH affect oil extraction in different ways, depending on rock composition, in some cases promoting the dissolution of carbonates and under certain conditions promoting carbonate precipitation, mainly as calcite and dolomite (Belyaev et al., 2004; Voordouw, 2011). In any case, the pH is a parameter that must be considered for future applications.

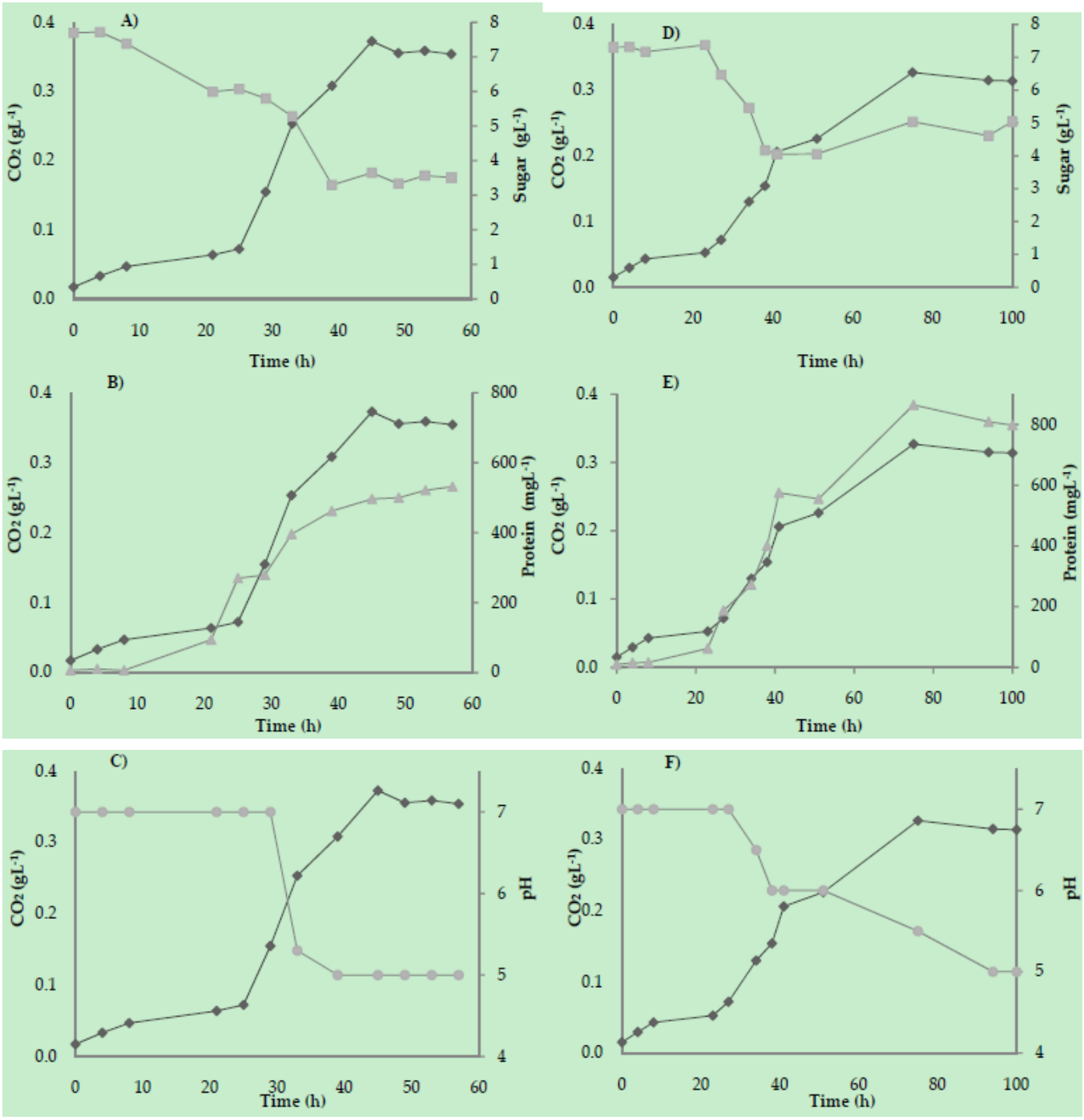

FIG.2 KINETIC STUDIES OF CULTURES NW O AND CW O IN SI MEDIUM AT 70°C. A, B AND C CORRESPOND TO NW O CULTURE EVALUATED DURING 57 H AND D, E, AND F TO CW O CULTURE DURING 100 H. BLACK DIAMONDS INDICATE PRODUCTION OF CO_2, GRAY TRIANGLES THE TOTAL PROTEIN CONCENTRATION, GRAY SQUARES THE RESIDUAL SUGAR, AND GRAY CIRCLES PH VALUES

Culture NW O showed exponential growth and CO_2 production from 25 to 45 h with a maximum production of 0.37 gL^{-1} of CO_2. This culture showed a yield of 102 mg CO_2 g^{-1} of sugar (Fig. 2A and 2B), while culture CW O showed an exponential growth phase from 23 to 75 h with a maximum production of CO_2 of 0.33 gL^{-1} and a yield of 66 mg CO_2 g^{-1} of sugar.

As shown in Figures 2A and 2D, sugar consumption is not complete: before microbial growth reaches the stationary phase, the remaining sugar value becomes constant; this occurs because sugar cane molasses contain between 45% and 50% of fermentable sugars which, are used depending on the efficiency of microbial process (Enriquez-Poy, 2005).

Effect of Reformulated Medium (SR) on Increase of CO_2 Production

To demonstrate an increase in CO_2 production, the assay was performed with culture NW O at 70°C, and accumulated CO_2 was evaluated during 143 h of incubation in both SI and SR media. As shown in Figure 3, a maximum microbial CO_2 production was obtained with SR medium of 3.13 g L^{-1} after 143 h of incubation, whereas with SI medium a production of 1.64 g L^{-1} was observed. CO_2 production increased significantly suggesting media reformulation generates appropriate conditions to fermentation.

Other studies have reported the use of microorganisms for CO_2 production to MEOR technologies. *Clostridium tyrobutiricum*, known for its industrial applications in the production of CO_2, especially in the food industry, was evaluated at different salinities, close to those reported in oil reservoirs; the results showed a high production of CO_2, up to 4.02 g L^{-1}, with resistance to different salinities, though under conventional temperature conditions (35°C), with less probability to survive under the temperature conditions of an oil well (Rudik and Sogaard, 2009). A recent study, performed under conditions close to those of oil reservoirs, showed that *Thermoanaerobacter* spp. generates 1.67 g of CO_2 per liter of culture medium, a yield similar to that seen in the present study (which was conducted without reformulation), and this concentration was enough to enhance the recovery of heavy oil from carbonate porous media by up to 12% (Castorena-Cortés et al., 2012).

Microbial enhanced oil recovery is an emerging technology, enjoying increasing interest due to its economical, ecological, and operational advantages. Most oil-field tests have involved water and chemicals injection, with cessation of flow to allow reaction; this, obviously, entails an interruption of production for a considerable period, so companies prefer different enhanced oil recovery (EOR) technologies (Thomas, 2008).

However, some success stories are changing our perspective on this. An example of this is the injection of 1-3 m^3 of concentrated nutrients to an oil well followed by a one-week cessation, which resulted in a doubling of the oil production rate throughout the next year (Town, 2009).

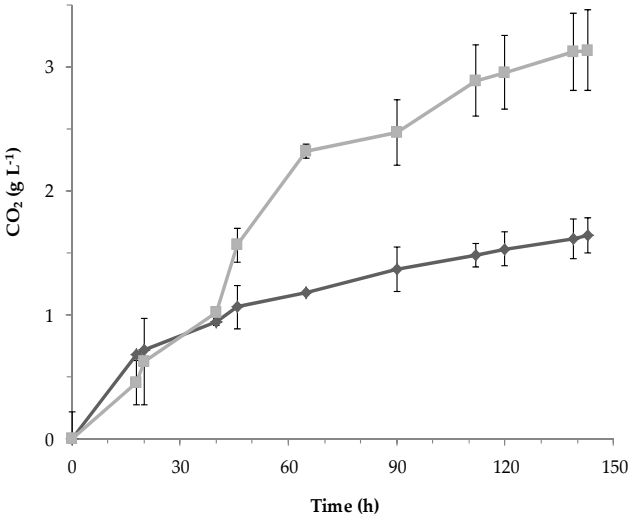

FIG. 3 CARBON DIOXIDE PRODUCTION BY CULTURE NW O IN SI (BLACK DIAMONDS) AND SR MEDIA (GREY SQUARES), AT 70°C DURING 165 H

Microbial Identification

Two ribosomal libraries were constructed, with 105 clones obtained for NW O and 77 clones for CW O. These clones were considered sufficient to represent the total species.

Table 3 shows and relates each representative clone with its closest-relative match in the database and phylogenetic affiliation. All sequences were related to species level. Of the 26 phylotypes, 65% correspond to *Thermoanaerobacterales* and 35% to *Thermotogales*.

To visualize the relationship between the ribosomal sequences derived from the oil samples, we constructed philogenetic trees by the neighbor-joining method. Sequences corresponding to *Thermotogales* and *Thermoanaerobacterales*, as well as sequences of related organisms found in the GenBank data base, are shown in Figures 4 and 5.

TABLE 3 PHYLOGENETIC RELATIONSHIP OF SELECTED CLONES.

Microbial group	Representative Clones	Phylogenetic Relationship	
		Closest Species in Gen bank (Accession Number)[A]/Similarity (%)[B]	**Microbial Affiliation**
Thermoanaerobacterales	2AF, 4AF, 7AF, 12AF, 15AF, 17AF, 24AF, 45AF, 18AF, 47AF	*Caldanaerobactersubterraneus subsp. yonseiensis*(219857468) / 99.4-99.8	*Caldanaerobactersubterraneus*
	4AF	*Caldanaerobactersubterraneussubsp.subterraneus*(FR749971) / 99.0	*Caldanaerobactersubterraneus*
	3C, 3LC, 9C, 21C, 22C, 30C, 34C	*Thermoanaerobacterpseudethanolicus* (167036431) / 98.8-99.2	*Thermoanaerobacterpseudethanolicus*
Thermotogales	11C, 18C, 23C, 32C, 35C, 39C, 41C, 47C, 50C	*Thermotoganeapolitana* (NR_027530) / 99.3-100	*Thermotoganeapolitana*

[A] The best match was selectedusing the closest sequence fromthe phylogenetic tree

[B] Similarity percentage was estimated by considering the number of nucleotide-substitutions between a pair of sequences divided by the total number of compared bases.

According to the results, fermentative microorganisms were identified as follows: the NW O culture is composed of the species *Thermoanaerobacter pseudethanolicus* and *Thermotoga neapolitana*, while culture CW O consists of *Caldanaerobacter subterraneus*.

Few previous works have reported on the microorganisms to be found in Mexican oil fields. Miranda-Tello et al. 2003 examined the metabolism of *Garciella nitratireducens*, a member of the *Clostridiales* order, to assess the possibility of effecting a major shift from sulfate reduction to nitrate reduction, as a means to counteract souring. *Petrotoga mexicana* is another microbial species originating from offshore platforms located in the Gulf of Mexico (Miranda-Tello et al., 2004), and recently members of the *Thermoanaerobacter* genus, identified using the variable V3 region of 16S rRNA, were found in cultures derived from oil samples from a platform in the San Felipe formation, Veracruz, Mexico (Castorena-Cortés et al., 2012).

Thermotogales have a broad range of metabolic capabilities, which may explain their widespread distribution and frequent detection in oil fields (Orphan et al., 2000). The *Thermotoga* genus ferments carbohydrates, forming H_2, CO_2, acetate, and lactic acid. However, in the presence of sulfate, instead of H_2, H_2S is formed, an undesirable metabolite in MEOR applications, due to its souring effect (Stetter and Huber, 1999).

Members of the genus *Thermotoga* have been detected in oil-reservoir samples around the world, suggesting that they belong to a natural microbial community in deep underground strata, because of their high growth temperatures (i.e., between 65°C to 90°C) and anaerobic metabolism (Magot et al., 2000).

Thermotoga neapolitana metabolizes a wide variety of carbohydrates; among the most important of these are: glucose, sucrose, starch, cellulose, and xylose. Cellulose and xylose are used by *Thermotoga maritime* as carbon sources for production of H_2, this biogas is of recent interest as an alternative energy source, and little is known about applications of H_2 in MEOR (Magot et al., 2000; Stteter and Huber, 1999).

The use of diverse carbohydrate sources is a special characteristic of the genus *Thermotoga***.** From the genome data one predicts that 7% of genes are involved in the use of carbon sources; also, they share with *Archaea* a large number of genes involved in the use of carbon sources, suggesting their acquisition by horizontal transference (Conners et al., 2006).

Another important group found in the present work was that belongs to *Thermoanaerobacterales*, another anaerobic heterotrophic fermentative bacterium. The *Thermoanaerobacter* genus has the ability of fermenting a wide variety of monomeric and polymeric carbohydrates, and to produce ethanol, another compound useful in MEOR technologies (Onyenwoke et al., 2007); large amounts of ethanol can be produced by consortia of *Thermoanaerobacter* and *Clostridium* species (Feng et al., 2009). In the *Thermoanaerobacter* genus there are mobile bacteria that ferment carbohydrates include xylose, cellobiose, starch, glucose, maltose, and sucrose. Their optimum growth temperature is 65°C, and their doubling time is about 75 min, important characteristics for some applications.

However, a possible disadvantage is their role in the reduction of thiosulfate to H_2S, which is involved in oil souring and corrosion (Orphan et al., 2000).

Caldanaerobacter subterraneus is a thermophilic bacterium, recently separated from the *Thermoanaerobacter* genus. *Caldanaerobacter subterraneus* has different subspecies. Metabolically it is an efficient fermenter of a wide range of carbon sources, producing acetate, L-alanine, lactate, H_2, and CO_2. Thiosulfate is reduced to elemental sulfur without production of H_2S, which is an advantage, compared with *Thermotoga* and *Thermoanaerobacter* species. In the presence of thiosulfate the amount of acetate produced per mole of glucose increases, suggesting a shift in the use of electron acceptors during the metabolism of carbohydrates (Fardeau et al., 2005).

Oil recovery enhanced by microbially produced CO_2 is still in the research stage, but injection of abiotic CO_2 has been a successful technology for many years. Compared to other tertiary recovery methods, CO_2 has the potential to enter into zones without the invasion of water previous and thus releasing the trapped oil which cannot be extracted by conventional methods. The CO_2 requirement for EOR is in the order of 1 to 3 tons of CO_2 per ton of oil produced, depending on both reservoir and oil characteristics (Jaramillo et al., 2009).

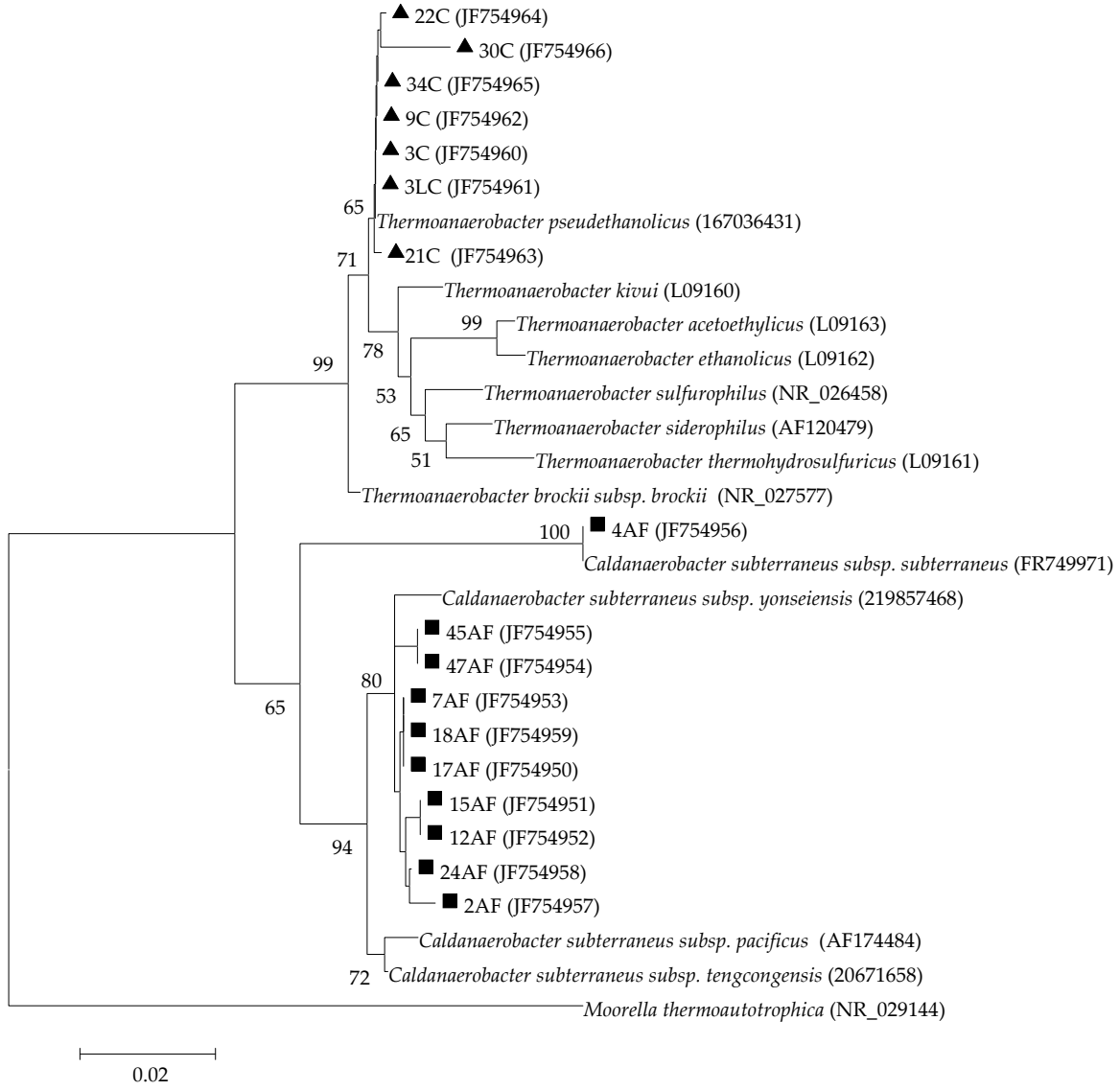

FIG. 4 NEIGHBOR-JOINING PHYLOGENETIC TREE OF 16S RRNA GENE SEQUENCES FROM CONSORTIA NW O (BLACK TRIANGLE) AND CONSORTIA CW O (BLACK SQUARES). THE SCALE BAR INDICATES THE NUCLEOTIDE SUBSTITUTIONS PER SITE. NUMBER AT THE BRANCHES INDICATES THE BOOTSTRAP VALUES OF 1,000 RESAMPLING. *Moorellathermoautotrophica* SERVED AS OUT-GROUP.

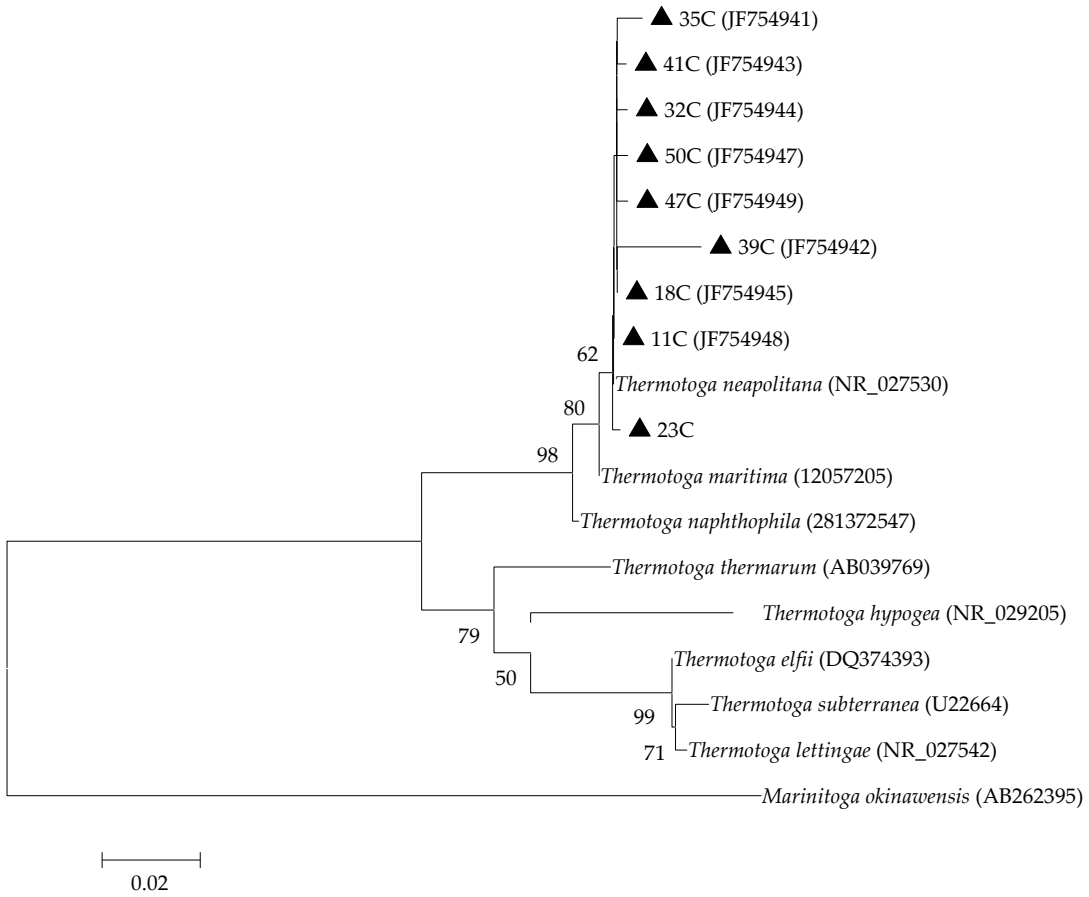

FIG. 5 PHYLOGENETIC TREE OF 16S RRNA GENE SEQUENCES CLONED FROM CONSORTIA NW O (BLACK TRIANGLE). DISTANCES WERE CALCULATED WITH THE KIMURA 2-PARAMETER SUBSTITUTION MODEL. THE SCALE BAR INDICATES THE NUCLEOTIDE SUBSTITUTIONS PER SITE. NUMBERS AT THE BRANCHING POINTS INDICATE THE BOOTSTRAP VALUES OF 1,000 RESAMPLING. *Marinitogaokinawensis* SERVED AS OUT-GROUP

CO_2 requirements for applications are related to dispersion phenomena, and with operational aspects, e.g. whether processes are continuous, in batch, or *Huff 'n' Puff* (Thomas, 2008). For testing *Huff 'n' Puff*, high-volume runs with 80 to 2 600 tons of CO_2 (1.5 to 50 million standard cubic feet) have been proposed, generating an increase in the recovery from 5 to 20 000 oil barrels (bbl) (Enick and Olsen, 2012; Grigg et al., 2005). In the present work we obtained a maximum output of 0.5 g CO_2 per liter per day at 70°C at 35 g L^{-1} of NaCl, which compared with abiotic injection (≈ 1.88 g L^{-1} CO_2 per day) is a limited production of gas; however, the microbial production of CO_2 has other advantages: microorganisms can move through the reservoir, and metabolism produces CO_2 continuously depending on availability of fermentative carbohydrates and microbial adaptation. Additional benefits of the biological production of CO_2 are that it does not require trapping mechanisms, transportation, purification, storage, nor continuous injection, processes that consume time, energy, and money (Rudick and Sogaard, 2009).

Conclusions

Fermentative microorganisms from Mexican oil fields were selected for their CO_2-production using molasses as carbon source. The reformulation of the medium allowed an increased production of carbon dioxide. Microbial cultures were identified as *Thermotoga neapolitana*, *Thermoanaerobacter pseudethanolicus*, and *Caldanaerobacter subterraneus*. These findings are important because these microbial cultures could be proposed as excellent candidates for MEOR applications.

ACKNOWLEDGMENTS

We are grateful for the assistance provided by Rafael Martínez de la Paz (CICATA Qro.) and Graciela García Caloca (IMP).

REFERENCES

Altschul, S.F., Gish, W., Miller, W., Myers E.W. and Lipman, D.J., "Basic local alignment search tool", *J. Mol. Biol.*, 1990, vol. 215, pp. 403–410.

Belyaev, S. et al., "Use of microorganisms in the biotechnology for the enhancement of oil recovery". *Microbiology*, 2004, vol. 73, pp. 590–598. Translated from *Mikrobiologiya,* vol. 73, pp. 687–697.

Bermúdez, J. et al., "Diagenetic history of the turbidity clitharenites of Chicontepec Formation, northern Veracruz: controls on the secondary porosity for hydrocarbon emplacement: Gulf Coast" *Association of Geological Societies Transactions*, 2006, vol. 56, pp. 65-72.

Bonch-Osmolovskaya, E.A. et al., "Radioisotopic, culture-based, and oligonucleotide microchip analyses of thermophilic microbial communities in a continental high-temperature petroleum reservoir", *Appl. Environ. Microbiol.*, 2003, vol. 69, pp. 6143-6151.

Bradford, M.M., "A rapid and sensitive method for the quantitation of microgram quantities of protein utilizing the principle of protein-dye binding", *Anal. Biochem.,* 1976, vol. 72, pp. 248–254.

Bryant, R.S. and Burchfield,T.E. "Review of microbial technology for improving oil recovery", *SPE Reservoir Eng. J.*, 1989, vol. 4, pp. 151-154.

Castorena-Cortés, G. et al.,"Evaluation of indigenous anaerobic microorganisms from mexican carbonate reservoirs with potential MEOR application", *J. Petrol.Sci. Eng.*, 2012, vol. 81, pp. 86-93.

CNH, Comisión Nacional de Hidrocarburos, "Informe 2010, Proyecto Aceite Terciario del Golfo", Primera revisión y recomendaciones.

Conners, S.B. et al., "Microbial biochemistry, physiology, and biotechnology of hyperthermophilic *Thermotoga* species", *FEMS Microbiol. Rev.*, 2006, vol. 30, pp. 872–905.

Dahle, H., Garsho, F., Madsen, M. and Birkeland, N.K., "Microbial community structure analysis of produced water from a high-temperature North Sea oil-field", *Antonie van Leeuwenhoek*, 2008, vol. 93, pp. 37-49.

Donaldson, E.C. and Clark, J.B., "Conference focuses on microbial enhancement of oil recovery", *Oil Gas J.,* 1982, vol. 82, pp. 47-49.

DuBois, M., Gilles, K.A., Hamilton, J.K., Rebers P.A. and Smith, F. , "Colorimetric method for determination of sugars and related substances", *Anal. Chem.*, 1956, vol, 28, pp. 350–356.

EnickR.M. and Olsen, D.K., "Mobility and Conformance Control for Carbon Dioxide Enhanced Oil Recovery (CO_2-EOR) via Thickeners, Foams, and Gels A Detailed Literature Review of 40 Years of Research and Pilot test", *Society of Petroleum Engineers,* SPE Improved Oil Recovery Symposium, 2012.

Enriquez-Poy, M., "Producción de etanol anhidro en los ingenios azucareros", short communication, *CONAE,* 2005, México.

Fardeau, M.L. et al., "*Thermoanaerobacter subterraneus* sp. nov., a novel thermophile isolated from oilfield water", *Int. J. Syst. Evol. Microbiol.,* 2000, vol. 50, pp. 2141–2149.

Feng, X. et al., "Characterization of the Central Metabolic Pathways in *Thermoanaerobacter* sp. Strain X514 via Isotopomer-Assisted Metabolite Analysis", *Appl. Environ. Microbiol.,* 2009, vol. 75, pp. 5001–5008.

Gachuz-Muro, H. and Sellami, H., "Analogous Reservoirs to Chicontepec, Alternatives of Explotation for this Mexican Oil Field", *Society of Petroleum Engineers*, 2009, EUROPEC/EAGE Conference and Exhibition, pp. 1-13.

Galtier, N., Gouy, M. and Gautier, C., "SEA VIEW and PHYLO_WIN: two graphic tools for sequence alignment and molecular phylogeny", *Comput. Appl. Biosci.*, 1996, vol. 12, pp. 543–548.

Grigg, R.B., Svec, R.K.,Zeng, Z.W., Bai, B. and Liu, Y., "Improving CO_2 Efficiency for Recovering Oil in Heterogeneous Reservoirs", Final Report New Mexico Petroleum Recovery Research Center, New Mexico Institute of Mining and Technology. DOE Contract NO. DE-FG26-01BC15364, 2005, pp.27-53.

Hall, T.A., "BioEdit: a user-friendly biological sequence alignment editor and analysis program for Windows 95/ 98/NT", *Nucleic Acids Symp Ser.*, 1999, vol. 41, pp. 95–98.

Head, I.M., Jones D.M. and Larter, S.R., "Biological activity in the deep subsurface and the origin of heavy oil", *Nature*, 2003, vol. 426, pp. 344–352.

Hillis D.M. and Bull, J.J., "An empirical test of bootstrapping as a method for assessing confidence in phylogenetic analysis", *Syst. Biol.*, 1993, vol. 42, pp. 182–192.

Jack, T.R., "Enhanced oil recovery by microbial action", In Yen, T.F., Kawahara, F.K. and Hertzberg, R. (eds.), Chemical and Geochemical Aspects of Fossil Energy Extraction, 1982, Ann Arbor, MI. Ann Arbor Science.

Jaramillo, P., Griffin, W.M. and McCoy, S.T., "Life cycle Inventory of CO_2 in an Enhanced oil recovery", *Environ. Sci. Technol.,* 2009, vol. 43, pp. 8027-8032.

López-Ramírez, S. "Investigación complementaria para mejorar la recuperación de aceite por vía microbiana", Informe adopción, desarrollo y adaptación de tecnologías aplicadas a la recuperación de aceite pesado, Proyecto facturable, IMP 43461, 2005.

Magot, M., Ollivier, B. and Patel, B.K.C., "Microbiology of petroleum reservoirs". *Antonie van Leeuwenhoek*, 2000, vol. 77, pp. 103–116.

Miranda-Tello, E. et al., "*Garciella nitratireducens* gen. nov., sp. nov., an anaerobic, thermophilic, nitrate- and thiosulfate-reducing bacterium isolated from an oil field separator in the Gulf of Mexico", *Int. J. Syst. Evol. Microbiol.,* 2003, vol. 53, pp. 1509-1514.

Miranda-Tello, E, et al., "*Petrotoga mexicana* sp. nov., a novel thermophilic, anaerobic and xylanolytic bacterium isolated from an oil-producing well in the Gulf of Mexico", *Int. J. Syst. Evol. Microbiol.,* 2004, vol. 54, pp. 169–174.

Onyenwoke, R.U., Kevbrin, V.V., Lysenko, A.M. and Wiegel, J., "*Thermoanaerobacter pseudethanolicus* sp. nov., a thermophilic heterotrophic anaerobe from Yellowstone National Park", *Int. J. Syst. Evol. Microbiol.,* 2007, vol. 57, pp. 2191–2193.

Orphan, V., Taylor, L., Hafenbrandl, D.and Delong, E., "Culture-dependent and culture-independent characterization of microbial assemblages associated with high-temperature petroleum reservoirs", *Appl. Environ. Microbiol.*, 2000, vol. 66, pp. 700-711.

PEMEX, Exploración y Producción, Informe 2011, Las reservas de hidrocarburos de México.

Rafique M.A. and Ali, U., "Microbial Enhanced Oil Recovery (MEOR) with special emphasis to the Uneconomical Reserves", SPE Indian oil and Gas Technical Conference and Exhibition, 2008, Mumbai, India.

Relman, D. A., "Universal bacterial 16S rDNA amplification and sequencing", in Persing, D. H., Smith, T. F., Tenover, F. C. and White, T. J., Diagnostic molecular microbiology: principles and applications, American Society of Microbiology, 1993, pp. 489-496.

Rosselló-Mora, R. and Amann, R., "The species concept for prokaryotes". *FEMS Microbiol. Rev*., 2001, vol. 25, pp. 39–67.

Rudik, S. and Sogaard, E., "How specific microbial communities benefit the oil industry Microbial Enhanced oil recovery (MEOR)". In Whitby, C., Applied Microbiology and Molecular Biology in oilfield systems. Proceedings from the International Symposium on Applied Microbiology and Molecular Biology in oil Systems (IMOS-2). 2009, pp. 179-187.

Sambrook J. and Russell, D.W. "Molecular cloning: a laboratory manual". Cold Spring Harbor Laboratory Press. 3rd Edition. China. 2001.

Sen, R., "Biotechnology in petroleum recovery: The microbial EOR", *Progress in Energy and Combustion Science*, 2008, vol. 34, pp. 714-724.

Stetter, K. and Huber, R., "The role of hyperthermophilic prokaryotes in oil fields, Microbial Ecology of Oil Fields", In Bell, C.R., BrylinskyM. and Johnson-Green, P., Microbial Biosystems: New Frontiers, Proceedings of the 8th International Symposium on Microbial Ecology, 1999, Atlantic Canada Society for Microbial Ecology, Halifax, Canada.

Tamura, K., Peterson, D., Peterson, N., Stecher, G., Nei, M., and Kumar, S., "MEGA 5: Molecular Evolutionary Distance and Parsimony Methods", *Molecular Biology and Evolution*, 2011, vol. 28, pp. 2731-2739.

Thomas, S. "Enhanced Oil Recovery-An Overview", *Oil & Gas Sci. Technol.*, 2008, vol. 63, pp. 9-19.

Thompson, J.D., Gibson, T.J., Plewniak, F. Jeanmougin, F. and Higgins, D.G., "The CLUSTAL_X windows interface: flexible strategies for multiple sequence alignment aided by quality analysis tools", *Nucleic Acids Res.,* 1997, vol. 25, pp. 4876– 4882.

Torres, L.G., Muñoz, A., Avendaño, J.R. and Leharne, S., "Viscosity, surface tension and other physical-chemical characteristics of three crude oils arising from Chicontepec, Mexico". *J.Petrol.Sci.Technol.* In press. 2012.

Town, K., Energy, H., Sheehy, A.J. and Govreau, B.R., "MEOR success in southern Saskatchewan". *SPE Annual Technical conference and exhibition*, SPE 124319, 2009, New Orleans, Louisiana.

Voordouw, G. "Production-related petroleum microbiology: progress and prospects", *Curr. Opin. Biotechnol.*, 2011, vol. 22, pp. 401-405.

Wolicka, D. Borkowski, A. and Dobrzynski, D., "Interactions between microorganisms, crude oil and formation waters", *Geomicrobiol. J.*, 2010, vol. 27, pp. 43-52.

Regina Hernández-Gama Jalisco, Mexico, 1982, student of PhD in Bioprocesses, UPIBI-IPN, Mexico. Master in Chemical and Biological Sciences, ENCB-IPN, Mexico, 2008. She has experience in: (a) Microbial ecology, (b) Microbial diversity and (c) Microbial enhanced oil recovery.

She works as Associated Professor at CICATA-IPN, Queretaro, Mexico, recent international paper: Navarro-Noya, Y.E., Jan-Roblero, J., Gonzalez-Chavez, M.C., Hernandez-Gama, R., Hernandez-Rodriguez, C. Bacterial communities associated with the rhizosphere of pioneer plants (Bahia xylopoda and Viguieralinearis) growing on heavy metals-contaminated soils. Antonie van Leeuwenhoek: Volume 97, Issue 4 (2010), Page 335-349. She has 1 paper at Mexican journal and 2 book chapters. She has directed 2 thesis at bachelors level.

Luis G. Torres has experience in industrial wastewaters' biological treatment and characterization/ remediation of metal and/or petroleum-contaminated soils. Currently, he has focused his interest on surfactant application to environmental problems. His main research lines are (a) surfactant-enhanced biodegradation of aged petroleum fractions in soils, (b) in-situ and ex-situ soil washing, and (c) preparation of petroleum fractions surfactant-water emulsions as a first step forfuel's biotreatments (e.g., biodesulfurization).

He has developed research stays in Laval University, Canada, ICIDCA-Habana, Cuba, University of Birmingham, UK (2), University of Greenwich at Medways, UK (2). He has more than 65 international publications in peer-reviewed journals. At the time he has directed more than 30 thesis, including PhD, master and bachelors levels. He is a National researcher (SNI) Level 2.

Norma G. Rojas-Avelizapa Cordoba Veracruz, Mexico, 1969. Ph. D. in Biotechnology, CINVESTAV, Mexico, 1999.M. Sc. in Biotechnology, CINVESTAV, Mexico City, Mexico, 1995. Industrial Chemist, Facultad de Ciencias Quimicas, Universidad Veracruzana, Mexico, 1995.

She is a Main Professor since 1995 at CICATA-IPN, Queretaro, Mexico. From 2008-2011, she was Postgraduate Coordinator of M.Sc. and Ph.D. in Advanced Technology at CICATA-IPN. From 1999–2005, she worked at Instituto Mexicano del Petroleo. Most relevant publication include Cervantes-Gonzalez, E., Rojas-Avelizapa, N.R., Cruz-Camarillo, R., García-Mena, J., Rojas-Avelizapa, L.I., (2009). Effects of keratinous waste addition on improvement of crude oil hydrocarbon removal by a hydrocarbon-degrading and keratinolytic mixed culture. International Biodegradation and Biodeterioration. 63: 1018-1022; Ramirez, M.E., Zapién, B., Zegarra, H.G., Rojas, N.G., Fernández, L.C., (2009) Assessment of hydrocarbon biodegradability in clayed and weathered polluted soils. International Biodegradation and Biodeterioration. 63: 347-353; Cervantes-Gonzalez, E. Rojas-Avelizapa, N.G. Cruz-Camarillo, R., García-Mena, J., Rojas-Avelizapa, L.I. (2008). Oil-removal enhancement in media with keratinous or chitinous wastes by hydrocarbon-degrading bacteria isolated from oil-polluted soils. Environmental Technology 29: 171-182. Current and previous research interests include (a) Microbial waste treatment, (b) Soil bioremediation and (c) Microbial enhanced oil recovery.

Dra Rojas is National researcher (SNI) Level 1.since 1999, is fellowship of EDI and COFAA. Accredited reviewer of CONACYT for national and international Grants. Founder member of Editorial Committee of UNACAR Tecnociencia Journal.

Effect of Brine Composition on CO_2/Limestone Rock Interactions during CO_2 Sequestration

Ibrahim Mohamed[*1],Jia He[2],and Hisham A. Nasr-El-Din[3]

[1]Advantek International Corp. [*]*Formerly with Texas A&M University*

Houston, Texas, USA 77063.

[2, 3]Texas A&M University, Petroleum Engineering Department
College Station, Texas, USA 77843

[*1]IMohamed@ADVNTK.com; [2]Jia.He@PE.TAMU.edu; [3]Hisham.Nasreldin@PE.TAMU.edu

Abstract

Several parameters affect the chemical reactions between CO_2/fluid/rock: pressure, temperature, rock type, and brine composition. Brine composition includes salt concentration and type. Pink Desert limestone cores were used to conduct a series of coreflood experiments to address the effect of brine composition on the chemical reactions between carbonic acid and limestone rock.

The experiments were designed to simulate the water alternating gas (WAG) injection of CO_2 into saline carbonate aquifers. Supercritical CO_2 and brines were injected at flow rates of 2 and 5 cm^3/min at 70 and 200°F. Seawater, formation brine, calcium chloride, sodium chloride, and magnesium chloride brines were used in this study.

A commercial compositional simulator was used to simulate the coreflood experiments at the lab conditions. The reaction rate constant of CO_2 with calcite at different brine compositions was adjusted to match the calcium concentration obtained in the lab.

Experimental data was used to predict the reaction rate constant between CO_2/brine/rock and found to be increasing as the brine salinity increased ($Log(k_{25})$= -9.2) when CO_2 dissolves in DI water, and -6.2 when CO_2 dissolves in 5 wt% $CaCl_2$ brine). A simulation study conducted on field scale showed that after 30 years of CO_2 injection and 1400 years after injection stopped, brine composition does not affect the trapping mechanism of CO_2 in the aquifer.

Keywords

CO_2 Sequestration; Coreflood Experiments; CO_2 Injection Modeling; CO_2/Brine/Rock Chemical Reactions

Introduction

The primary factor affecting well performance during CO_2 injection is rock type (carbonate or sandstone). For example, solution channels can be formed in limestone, creating a dominant flow path significantly altering flow behaviour (Grigg and Svec 2008). Increases in Ca^{2+}, Mg^{2+}, HCO_3^-, and CO_2 concentrations were noticed during monitoring, and the produced aqueous fluids and gases confirms the dissolution effect noted during CO_2 injection (Raistrick et al. 2009). Brine salinity and composition play a key role in the chemical reaction between CO_2/water/rock during CO_2 sequestration, since the total dissolved solids (TDS) affects the solubility of CO_2 in brines.

CO_2 is an acidic gas that dissolves in formation brine forming weak carbonic acid. Carbonic acid dissolves carbonate rocks forming calcium bicarbonate ($Ca(HCO_3)_2$). When the formation brine or the displacement brine contains SO_4^{2-}, calcium sulfate can precipitate (Egermann et al. 2005).

Krumhansl et al. (2002) concluded that with continuous dissolution of calcite, calcium saturation will increase and calcium sulfate precipitation will take place inside the core. This kind of precipitation is temperature dependent. At temperatures lower than 40°C, gypsum is the stable form, while at higher temperatures, anhydrite is the stable product. Hemihydrate is a metastable phase (Meijer and Van Rosmalen 1984).

The objective of this paper is to study the effect of brine composition on the chemical reactions between CO_2 and the formation lithology during WAG injection of CO_2 into a limestone aquifer. Furthermore, the impact of flow rate and temperature, on the final permeability has been studied. NaCl, $CaCl_2$, and $MgCl_2$ were tested at various concentrations (0, 1, 5, and 10 wt%). The reaction kinetics were obtained using a compositional simulator CMG-GEM (Generalized Equation-of-State Model) for each brine used in the current study.

Solubility of Calcium Sulfate

Solubility of calcium sulfate in brines is mainly controlled by the molecular hydration state. The solubility is also affected by temperature and brine salinity. The first solubility plot of calcium sulfate was published by Partridge and White (1929); their results showed that the solubility of anhydrite and hemihydrate in distilled water decreases as temperature increases. While gypsum solubility in distilled water increases as temperature increases up to 38°C, at higher temperatures solubility of gypsum decreases as temperature increases.

Meijer and Van Rosmalen (1984) used a computer program developed by Marshall and Sulsher (1968) to calculate the solubility of calcium sulfate in seawater. Their results showed that the solubility in seawater is higher than the solubility in distilled water, although temperature has the same effect on the solubility of calcium sulfate for both cases. Solubility of calcium sulfate decreases significantly as the total dissolved solid content approaches twice than that of seawater (Flint 1967).

Solubility of CO_2 in Brines

The effect of dissolved solids on the CO_2 solubility in water was studied by Enick and Klara (1989). They developed a correlation to calculate the solubility of CO_2 in brine that is applicable at reservoir conditions, taking into consideration the effect of dissolved solids. They assumed that solubility only depended on TDS, regardless of the type of salt.

The solubility of CO_2 in distilled water, NaCl and $CaCl_2$ brines used in the present study, at a pressure of 1300 psi and temperature of 200°F, was obtained from Nighswander et al. (1989), Duan et al. (2006), and Prutton and Savage (1945). Their work was specified for NaCl and $CaCl_2$ brines, while the solubility of CO_2 in $MgCl_2$ brines was calculated using the equation developed by Enick and Klara (1989) and is given in Table 1.

TABLE 1 CO_2 SOLUBILITY AT 1300 PSI AND 200°F

Salt Concentration, wt%	**0**	**1**	**5**	**10**
Brine Composition	**CO_2 Solubility, weight fraction**			
NaCl	0.0134	0.0130	0.0115	0.0098
$CaCl_2$		0.0130	0.0115	0.0096
$MgCl_2$		0.0128	0.0105	0.0083

Reaction Kinetics

The rate laws for mineral dissolution and precipitation for the chemical reactions between CO_2/brine/limestone are (Bethke 1996):

$$r_\beta = k_\beta A_\beta \left[1 - \left(\frac{Q_\beta}{K_\beta}\right)\right] \quad (1)$$

$$k_\beta = k_{0\beta} \exp\left[-\frac{E_{a\beta}}{R}\left(\frac{1}{T} - \frac{1}{T_0}\right)\right] \quad (2)$$

Where;

A_β = reactive surface area for mineral β, m²
$E_{a\beta}$ = activation energy for reaction of CO_2 with mineral β, J/mol
K_β = chemical equilibrium constant
$k_{0\beta}$ = rate constant of reaction of CO_2 with mineral β at a reference temperature T_0, mol/m².s
k_β = rate constant of reaction of CO_2 with mineral β at temperature T, mol/m².s
Q_β = ion activity product
R = universal gas constant = 8.31 J/mol.°K
r_β = Reaction rate, mole/m².s
T = temperature, °K

TABLE 2 LIST OF KINETIC RATE PARAMETERS FOR REACTIONS BETWEEN CO_2 AND LIMESTONE

Reference	**Log(ko) mol/m².sec**	**Ea KJ/mol*°K**	**Reference Temperature °C**	**Brine Composition**	
				Ion	**Conc. mg/l**
Gaus et al. (2004)	-6.35		37	Al	9.47E-04
				Ba	1.72
				C	0.83
				Ca	7093.88
				Cl	16982.08
				Fe	0.02
				K	5.55
				Mg	269.79
				Na	2436.92
				S	15.42
				Si	7.08
Bacon et al. (2009)	-1.69	23.5	54	Na	55152.53
				Mg	3038.13
				Al	0.01
				SiO_2	7.21
				K	18258.91
				Ca	30240.00
				Mn	2.20
				Fe	0.56
				Cl	125007.98
				SO_4	158.50
				HCO3	134.24
Sorensen et al. (2009)	-6.19	62.76	25	10 wt% NaCl	
Lee and Morse (1999)	-8.94		25	Na	91.60
				Ca	40.00
				Cl	141.37
				HCO_3	122.00

Reference	Log(ko) mol/m².sec	Ea KJ/mol*°K	Reference Temperature °C	Brine Composition	
				Ion	Conc. mg/l
Wellman et al. (2003)	-2.00		25	Na	16,575.65
				SO_4	629.21
				Mg	631.93
				Cl	29,993.41
				Ca	1,824.00
Knauss et al. (2005)	-6.19	62.7	25	Al	8.70E-04
				Ba	59.18
				Sr	109.44
				Ca	2,211.64
				Fe	36.28
				K	414.21
				Mg	461.82
				Na	40,845.98
				SiO_2	24.11
				Cl	68,757.94
				SO_4	10.32
Cantucci et al. (2009)	-5.81	23.5	25	Na	42,990.93
				K	2,502.29
				Ca	39.48
				Mg	0.16
				HCO_3	447.25
				Cl	63,815.76
				HS	3,261.04
				SO_4	4.44
				Li	2.57
				Sr	46.88
				Si	10.44
				Al	1.84E-03
Xu et al. (2006)	-6.19	62.76	25	Ca	7,284.00
				Mg	112.05
				Na	27,886.63
				K	2,807.26
				Fe	0.08
				Cl	60,979.50
				SiO_2	210.30
				HCO_3	457.63
				SO_4	194.05
				Al	1.53E-04
				Pb	2.07E-07
Wigand et al (2009)	-1.69	23.5	25	Al	0.08
				SiO_2	4.27
				Ca	275.48
				Fe	17.98
				K	64.00
				Mg	39.01
				Mn	47.03
				Zn	1.83
				Li	0.02
				Sc	0.16
				Cu	0.95
				Rb	0.07
				Sr	0.44
				Cd	0.02
				Pb	0.02

Different values for k_o between carbonic acid and calcite were reported in the literature (Alkattan et al. 1998). A summary of k_o and E_a used in previous studies with different brine compositions is given in Table 2. Log(k_o) ranged from -8.94 at a low salinity brine with TDS of 395 mg/l (Lee and Morse 1999), to -1.69 for a high salinity formation brine with TDS of 232,000 mg/l (Bacon et al. 2009).

Experimental Studies

Materials

Cylindrical Pink Desert limestone cores were used in this study with dimensions of 6 in. length and 1.5 in. diameter. the cores permeability and porosity are summarized in Table 3.

TABLE 3 PROPERTIES OF THE PINK DESERT CORES AND COREFLOOD EXPERIMENTS

Core #	Porosity (vol%)	Perme-ability (mD)	Temp-erature (°F)	Injection flow rate of CO_2 and brine (cm^3/min)	Brine Injected
1	19.6	61.8	200	2	Seawater without Sulfate
2	21.9	50.0	200	2	Seawater
3	18.9	56.52	70	2	Seawater
4	19.8	79.8	200	5	Seawater without Sulfate
5	22.4	77.0	200	5	Seawater
6	22.4	68.2	200	2	Formation Brine
7	19.6	57.5	70	2	Formation Brine
8	27.1	96.0	200	5	Distilled Water
9	24.1	77.0	200	5	1 wt% NaCl
10	24.4	99.0	200	5	5 wt% NaCl
11	24.4	99.0	200	5	10 wt% NaCl
12	25.9	93.5	200	5	1 wt% $CaCl_2$
13	24.7	91.0	200	5	5 wt% $CaCl_2$
14	26.9	85.0	200	5	10 wt% $CaCl_2$
15	26.2	80.0	200	5	1 wt% $MgCl_2$
16	23.6	72.0	200	5	5 wt% $MgCl_2$
17	24.8	93.0	200	5	10 wt% $MgCl_2$

CO_2 with purity of 99.8% (the impurities were mainly water vapor and nitrogen) was used in this study. Different synthetic brines were used; 1) equivalent to seawater excluding Na_2SO_4, 2) equivalent to seawater, and 3) equivalent to formation brine from the Middle East. The compositions of the three brines are given in Table 4. Bines that are composed of NaCl, $MgCl_2$, or

$CaCl_2$, at concentrations of 1, 5, and 10 wt% were also used. The density of the different brines were measured at room temperature using a DMA4100 density meter, and a PSL 1643/02 capillary viscometer was used to measure brine viscosity.

Coreflood Experiments

Seventeen coreflood experiments were conducted in this study. The experiments were run at temperatures of 70 and 200°F, and injection flow rates of 2 and 5 cm^3/min were used. A summary of the coreflood experiments is given in Table 3. More information about the coreflood setup was reported previously (Mohamed and Nasr-El-Din 2012).

TABLE 4 CONCENTRATIONS OF KEY IONS AND PROPERTIES OF SYNTHETIC BRINES

Ion	Seawater Without Sulfate	Seawater	Formation Brine
Cl^-	22,010*	22,010	143,285
SO_4^{2-}	0	2,850	108
Na^+	12,158	12,158	51,187
Mg^{2+}	1,315	1,315	4,264
Ca^{2+}	401	401	29,760
TDS, mg/l	35,884	38,734	228,604
Viscosity**, cP	1.040	1.045	1.70
Density**, g/cm^3	1.0260	1.0266	1.1640

*all concentrations are expressed in mg/l.
** measured at 70°F
pH ranges 6.4 to 6.9

Coreflood Procedure

1- The cores were dried in an oven at a temperature of 257°F for 5 hours, and then weighed.
2- The cores were saturated under vacuum with brine (brine composition depends on the experiment), and then weighed.
3- From the weight difference between the dry and saturated core and the brine density, the core porosity was calculated.
4- A core was placed inside the coreholder and brine was injected at room temperature until the pressure drop across the core stabilized. The core permeability was calculated using Darcy's law.
5- The system was heated up to the required temperature.
6- Start CO_2 injection at a constant flow rate for 5 pore volumes (CO_2 half cycle).
7- Alternate to brine for 5 pore volumes (brine half cycle).
8- Repeat steps 6 and 7 to reach the 3 WAG cycles.
9- Core effluent samples were collected throughout the experiment.
10- The concentrations of calcium, sodium, and magnesium ions were measured in the core effluent samples. Sulfate ion was measured when seawater was used.
11- A new core was used in each experiment.

Equipment

Calcium, sodium, and magnesium concentrations in the core effluent samples were measured using an AAnalyst 700-flame type. Sulfate concentration was measured using an Orbeco SP600 Spectrophometer, using the turbidity method based on precipitation with barium chloride.

Results and Discussion

WAG injection of CO_2 and seawater was conducted on cores #1-2 (seawater not containing sulfate for core #1, seawater with sulfate for core #2). Calcium concentration noted for core #1 was higher than the calcium concentration measured in the core effluent samples collected for core #2. Also, a reduction in the sulfate concentration was noted for core #2, which indicated that calcium sulfate precipitation occurred inside core #2.

Total amounts of calcium collected from cores #1 and 2 were 0.64 and 0.45 g, respectively, and the weight of the sulfate lost inside core #2 was 0.08 g (5.3% of the total weight of the injected sulfate). More damage was noted for core #2 because of calcium sulfate scales precipitated inside the core (permeability reduced from 50 to 43 mD). The change in the permeability for core #1 was negligible.

Effect of Temperature

Two temperatures (70 and 200°F) were tested to address the effect of calcium sulfate hydration form. Gypsum is the stable form at 70°F, and anhydrite is the stable form at 200°F. Fig. 1 shows that at 70°F (core #3) a higher calcium concentration was noted in the core effluent sample compared to core #2 (200°F). The solubility of gypsum at 70°F was found to be higher than the solubility of anhydrite at 200°F, 0.42 wt% for gypsum and 0.195 wt% for anhydrite (Flint 1967; Linnikov and Podbereznyi 1996), which explains the

higher concentration of sulfate noted for core #2 (the precipitation was less).

At the two temperatures examined in this study, the results showed that at the lower temperature (70°F) the solubility of calcium sulfate and CO_2 in seawater is higher, and more calcium carbonate dissolved, which resulted in an increase in the core permeability (from 56.5 to 60.6 mD). At the higher temperature (200°F) the solubility of calcium sulfate and CO_2 in seawater is less, which caused more precipitation and less calcium carbonate dissolution, which resulted in more damage noted to the core.

Effect of Injection Flow Rate

In this study, two flow rates were examined, 2 and 5 cm^3/min. A flow rate of 2 cm^3/min was discussed briefly in the previous section. Two coreflood experiments run at 5 cm^3/min, core #4 was run with no sulfate in the injected brine, and core #5 with sulfate in seawater composition, both were conducted at 200°F.

The injection flow rate of CO_2 did not have a significant effect on the core permeability after WAG injection of CO_2. The same behavior was noted when CO_2 was injected at 2 and 5 cm^3/min. Maximum calcium and minimum sulfate concentrations were similar at injection flow rates of 2 and 5 cm^3/min (Fig. 1). Precipitation of calcium sulfate was also evaluated by the change in the core permeability. For core #5, the permeability decreased from 77 to 69 mD; while it increased from 79.8 to 83 mD for core #4.

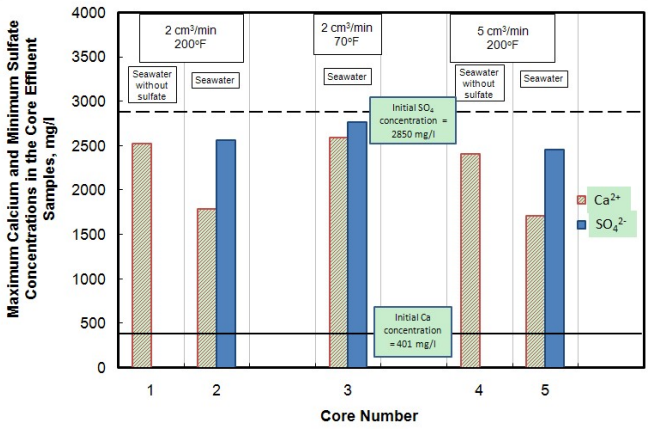

FIG. 1 MAXIMUM CALCIUM AND MINIMUM SULFATE CONCENTRATIONS IN THE CORE EFFLUENT SAMPLES FOR CORES #1-5

Effect of the High Salinity Formation Brine

Cores #6 and 7 were both flooded with CO_2 alternating formation brine at two different temperatures (70 and 200°F), the total dissolved solids for the formation brine used in this study was 228,604 mg/l (Alotaibi et al. 2010)

Fig. 2 shows that the increase in calcium concentration when formation brine is used in WAG injection is more pronounced when compared to seawater injection with CO_2. Calcium concentration increased from 29,760 mg/l initially to a maximum concentration of 60,000 mg/l during CO_2 injection at 200°F, and increased to 42,000 mg/l at 70°F.

The formation brine originally has low sulfate concentration, so the effect of the calcium sulfate scale was insignificant. The damage was mainly because of calcium carbonate precipitation as the calcium concentration noted in the core effluent sample was very high. Permeability of core #6 decreased from 68.2 to 64 mD, while for core #7, it increased from 57.5 to 63 mD.

Table 5 summarizes the change in the cores permeability, and Fig. 3 gives a brief summary of the total calcium collected in the core effluent samples and total sulfate precipitated for each experiment for cores #1-7.

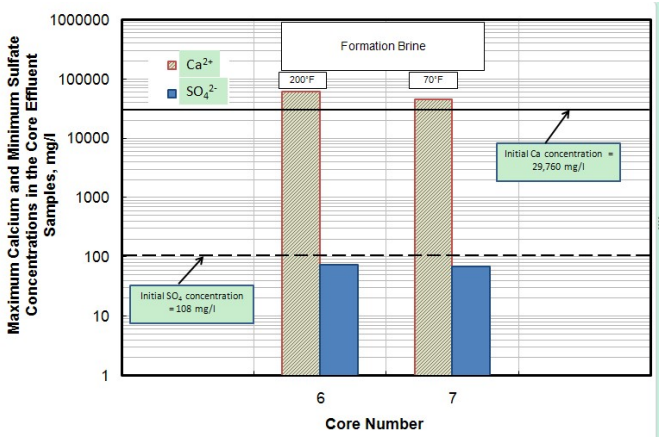

FIG. 2 MAXIMUM CALCIUM AND MINIMUM SULFATE CONCENTRATIONS IN THE CORE EFFLUENT SAMPLES FOR CORES #6-7

Effect of Brine Salinity

Effect of Deionized Water (DI Water)

Calcium concentration increased during CO_2 injection from 0 to 1080 mg/l due to rock dissolution, and a reduction in calcium concentration was observed during water injection to 500 mg/l. This behavior was repeated each cycle, with a slight change in the calcium concentration values. The maximum values were 1184 and 1070 mg/l, and the minimum values were 300 and 530 mg/l for the second and third cycles, respectively.

The total calcium collected from core #8 was 0.353 g. A reduction in the core permeability from 96 to 90 mD was observed after CO_2 injection.

Effect of NaCl Brines

Three coreflood experiments were run at NaCl concentrations of 1, 5, and 10 wt%. Measuring the permeability for these cores before and after CO_2 injection, showed no significant change in core permeability.

For 1 wt% NaCl brine, the maximum calcium concentration was almost the same as when distilled water was used (Fig. 4). The minimum calcium concentrations were 300 and 1000 mg/l for distilled water and 1 wt% NaCl brine, respectively. The maximum calcium concentrations were 1276, 1841, and 1700 mg/l, while the total calcium collected was 0.436, 0.635, and 0.54 g for 1, 5, and 10 wt% NaCl brine, respectively.

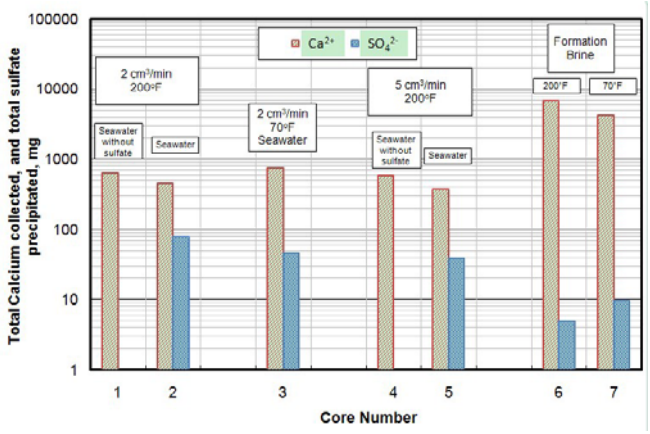

FIG. 3 TOTAL CALCIUM COLLECTED AND TOTAL SULFATE LOSS AS MEASURED IN THE CORE EFFLUENT SAMPLES.

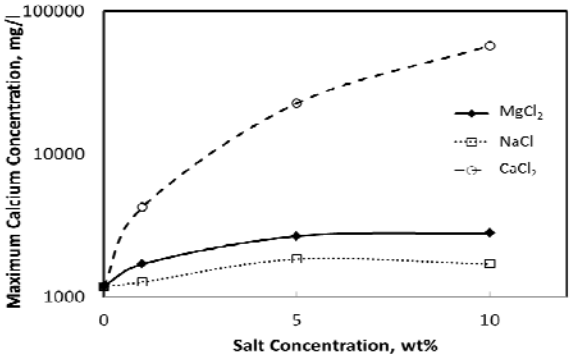

FIG. 4 MAXIMUM CALCIUM CONCENTRATION IN THE CORE EFFLUENT SAMPLES.

Effect of $CaCl_2$ Brines

Fig. 4 shows that for 1 wt% $CaCl_2$ brine, the maximum calcium concentration increased from 3100 mg/l initially to 4256 mg/l. This was an increase of 1156 mg/l, which was equal to the increase of calcium concentration when distilled water was used.

A significant increase in the calcium concentration in the core effluent samples was observed when increasing the concentration of calcium chloride in the injected brine. For 5 wt% $CaCl_2$ brine the calcium increased from 15,504 to a maximum concentration of 22,792, with a 7,288 mg/l increase in calcium concentration. When doubling calcium chloride concentration to 10 wt%, calcium increased from 31,008 to 57,000 mg/l, with 26,000 mg/l increase in calcium concentration. The total collected amounts of calcium were 0.32, 2.44, and 6.17 g for 1, 5, and 10 wt% $CaCl_2$ brine, respectively.

The ratio of the final core permeability to the initial permeability is given in Fig. 5. An enhancement in core permeability, of 6.5 %, was noted when 1 wt% $CaCl_2$ brine was injected, compared to 7 % loss in permeability when distilled water was used. At higher calcium chloride concentrations, 5 and 10 wt%, a permeability reduction of 14 % occurred after WAG injection of CO_2.

TABLE 5 EFFECT OF BRINE COMPOSITION ON THE CORE PERMEABILITY AFTER CO_2 WAG INJECTION

Core	$K_{initial}$ (mD)	K_{final} (mD)	Ratio	Injection Conditions	Brine
1	61.8	60.5	0.98	2 cm³/min 200°F	Seawater without sulfate
2	50	43	0.86		Seawater
3	56.5	60.6	1.07	2 cm³/min 70°F	Seawater
4	79.8	83	1.04	5 cm³/min 200°F	Seawater without sulfate
5	77	69	0.90		Seawater
6	68.22	64	0.94	200°F	Formation Brine
7	57.5	63	1.1	70°F	

A. *Effect of $MgCl_2$ Brines*

To examine the effect of magnesium chloride concentration on the core permeability during CO_2 sequestration, three coreflood experiments were run. Fig. 4 shows that with increasing the concentration of $MgCl_2$ in the injected brine, more calcium was collected in the core effluent samples. The maximum concentration of calcium detected in the samples were 1764, 2686, and 2843 mg/l for 1, 5, and 10 wt% $MgCl_2$

brine, respectively. Total amount of calcium collected was 0.477, 0.687, and 0.956 g. Magnesium concentration was the same for all core effluent samples.

Fig. 5 shows that as magnesium chloride concentration increased, the damage introduced to the cores was still close: 4, 5, and 8 % loss in the core permeability for 1, 5, and 10 wt% $MgCl_2$ brine, respectively.

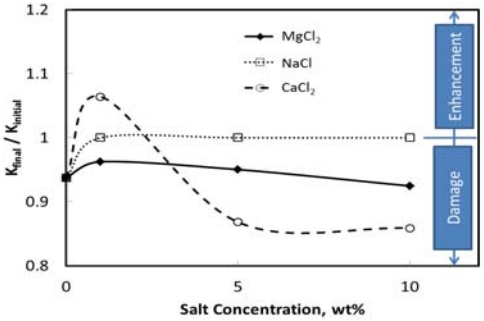

FIG. 5 CHANGE IN CORES PERMEABILITY WHEN DIFFERENT SALT CONCENTRATIONS OF NACL, $MgCl_2$, AND $CaCl_2$ BRINE WERE INJECTED IN CO_2 WAG INJECTION.

Simulation Studies

The experimental results showed that the kinetics of the reaction between CO_2 and limestone rock is a function in the brine composition. A compositional simulator (CMG-GEM) was used to predict the reaction rate constant between CO_2 and limestone for each brine used based on the calcium concentration measured in the core effluent samples. A field scale simulation was also run to address the effect of brine composition on the permeability distribution during WAG injection of CO_2.

The simulator input is: the injection schedule, CO_2 and brine relative permeability curves, capillary pressure between CO_2 and injected brine, kinetics of the chemical reactions between CO_2 and calcite, initial porosity and permeability, and the core dimensions.

To calculate the relative permeability curves, the irreducible water saturation and the critical saturation of CO_2 were obtained from the coreflood experiments. Relative permeabilities were calculated using Equations (3) and (4);

$$k_{rw} = 0.35\left(\frac{S_w - 0.25}{1 - 0.25}\right)^4 \quad (3)$$

$$k_{rCO2} = 0.05\left(\frac{S_{CO2} - 0.15}{1 - 0.15 - 0.25}\right)^{1.5} \quad (4)$$

Where;

k_{rw} = relative permeability to brine

k_{rCO2} = relative permeability to CO_2

S_w = brine saturation

S_{CO2} = CO_2 saturation

0.35 = relative permeability to brine at irreducible CO_2 saturation

0.05 = relative permeability to CO_2 at irreducible brine saturation

0.25 = irreducible brine saturation

0.15 = irreducible CO_2 saturation

The capillary pressure between CO_2 and brine was obtained using the model developed by El-Khatib (1995);

$$P_c = \frac{1}{\sqrt{2\tau}}\left(\frac{1}{\sqrt{2b+1}}\right)\left(\frac{(1-S_{wi})^{b+0.5}}{(S_w - S_{wi})^b}\right)\left(\frac{\sigma \ Cos\theta}{\sqrt{k/\phi}}\right) \quad (5)$$

Where;

B = saturation exponent

K = absolute permeability, m^2

P_c = capillary pressure, Pa

S_w = brine saturation

S_{wi} = irreducible brine saturation

T = tortuosity

Θ = contact angle

Σ = interfacial tension between CO_2 and brine, N/m

ϕ = porosity, fraction

El-Khatib (1995) gave an average value for the saturation exponent (b) to be 1.077. The tortuosity value was calculated based on the core porosity Equation (6) (Boving and Grathwohl 2001):

$$\tau = \varnothing^{-1.2} \quad (6)$$

Shariat et al. (2012) conducted a lab study to measure the interfacial tension between CO_2 and different brines, and the interfacial tension between CO_2 and seawater at the experimental conditions was found to be 0.0224 N/m. The contact angle between CO_2 and brine was adjusted in order to match the experimental results. Contact angle of 80° was found to give the best match for all cores used in the current study.

Core Scale Simulation

The cylindrical cores were divided into radial grids with 5X20X20 blocks in the radial coordinates r, Θ, and z directions, respectively. The initial permeability and porosity were assumed constant for all grid blocks, cores initial porosity and permeability are shown in Table 3.

The simulator uses Equations (1) and (2) to predict the dissolution and/or precipitation rate for calcium carbonate during the reaction with CO_2. In this paper, the activation energy of 62.7 KJ/mole.°K, and a reactive surface area of 9.5 cm^2/g were used for all cases (Svensson and Dreybrodt 1992). In order to simulate the calcium concentration obtained from the experimental study, the reaction rate constant was found ($\log(k_{25})$) to be in the range between -9.2 (for DI water case) and -6.2 (for 5 wt% $CaCl_2$ brine case). A summary for the reaction rate constant for all cases is given in Table 6. It is clear that at a higher salt content the reaction rate constant increases, and a larger value obtained for $CaCl_2$ brines than $MgCl_2$ brines, and a smaller value obtained for NaCl brines. The simulation failed at high calcium concentration cases (10 wt% $CaCl_2$ and formation brine), no reaction rate constant could be predicted for these cases.

The simulator also has the capability to predict the change in cores permeability due to the dissolution and precipitation reactions. The change in core porosity was calculated using Equation (7), while the permeability was calculated using Carman-Kozeny equation based on the initial and final porosity Equation (8):

$$\phi \equiv \phi_o - \sum_{\beta=1}^{n_m} \left(\frac{N_\beta}{\rho_\beta} - \frac{N^0{}_\beta}{\rho_\beta} \right) \quad (7)$$

$$k = k_o \left(\frac{\varphi}{\phi_o} \right)^m \left(\frac{1-\phi_o}{1-\phi} \right)^2 \quad (8)$$

Where;

K = Current permeability, mD
k_0 = Initial permeability, mD
m = Carman-Kozeny exponent
N_β = total moles of mineral β per bulk volume at the current time, mole/cm^3
$N^0{}_\beta$ = total moles of mineral β per bulk volume at the time 0, mole/cm^3
ϕ = Current porosity, fraction
ϕ_0 = Initial porosity, fraction
ϱ_β = mineral molar density, mole/cm^3

The permeability and porosity change distribution across the core calculated by CMG-GEM for cores #4 and 5 are shown by Figs. 6 and 7, respectively. The Carman-Kozeny exponents used in these calculations were 4.53 when seawater without sulfate injected with CO_2 during WAG injection, and 7.82 in the seawater case (Mohamed and Nasr-El-Din 2012).

Fig. 6 shows that for core #4 an enhancement in the permeability was noted close to the core inlet until 1.5 in. from the core inlet; more increase in the permeability was noted in each cycle. Behind this region, damage was noted at the core outlet, and the damage increased with the number of WAG cycles. Seawater in CO_2 WAG injection causes a reduction in core permeability throughout the core length, with more damage close to the core inlet due to calcium sulfate precipitation (Fig. 7). The damage increases as more WAG cycles are injected.

TABLE 6 A SUMMARY OF THE REACTION RATE CONSTANTS FOR EACH BRINE USED IN THIS STUDY

Brine	Log (k_{25}) mol/m^2.s	Maximum Calcium Concentration Measured mg/l	Maximum Calcium Concentration Simulated mg/l
DI Water	-9.20	1,184	1,168
1 wt% NaCl	-9.08	1,276	1,264
5 wt% NaCl	-7.38	1,841	1,788
10 wt% NaCl	-7.30	1,700	1,724
1 wt% $MgCl_2$	-7.3	1,764	1,776
5 wt% $MgCl_2$	-7.05	2,686	2,672
10 wt% $MgCl_2$	-6.55	2,843	2,832
1 wt% $CaCl_2$	-7.72	[a]4,256	4,276
5 wt% $CaCl_2$	-6.20	[b]22,792	23,000
Seawater without sulfate	-6.70	[c]2,300	2,240
Seawater	-6.46	1,780	1,800

a initial calcium concentration = 3,100 mg/l
b initial calcium concentration = 15,504 mg/l
c initial calcium concentration = 401 mg/l

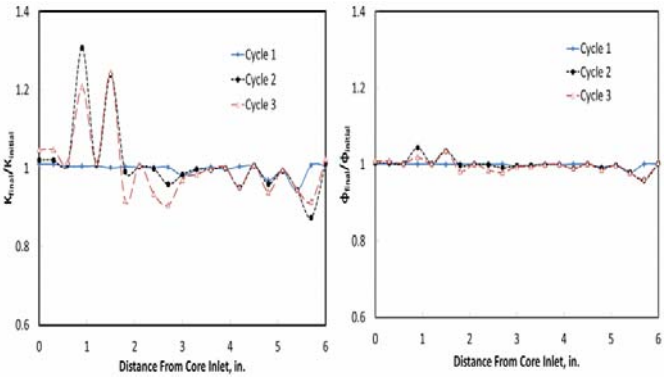

FIG. 6 PERMEABILITY AND POROSITY RATIOS AT THE END OF EACH WAG CYCLE WHEN WAG INJECTION OF CO_2 AND SEAWATER WITHOUT SULFATE CONDUCTED FOR CORE #4.

The overall core permeability after WAG injection for cores #4 and 5 is given in Fig. 8. Most of the change in permeability occurs during the first WAG cycle, the permeability after the second and third WAG cycle was almost the same as after the first cycle. A good match between the permeability measured in the lab and calculated by the simulator was also shown in Fig. 8.

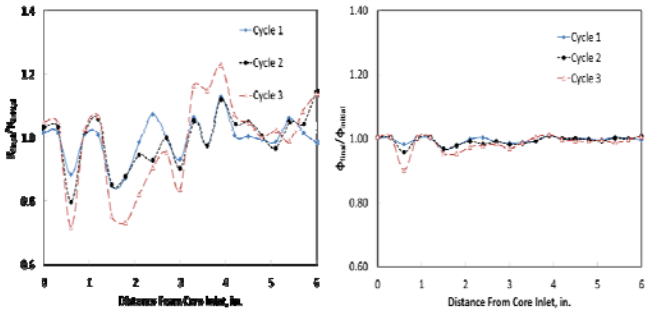

FIG. 7 PERMEABILITY AND POROSITY RATIOS AT THE END OF EACH WAG CYCLE WHEN WAG INJECTION OF CO_2 AND SEAWATER CONDUCTED FOR CORE #5.

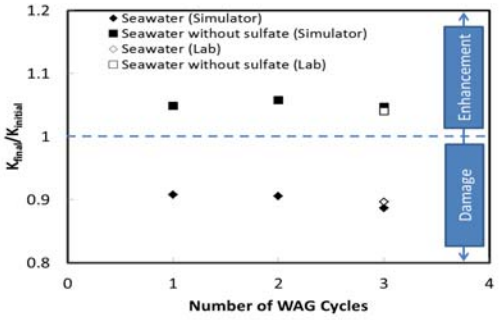

FIG. 8 COMPARISON BETWEEN THE PERMEABILITY DATA OBTAINED FROM THE SIMULATOR AND MEASURED IN THE LAB FOR CORES #4 AND 5.

A. *Field Scale Simulation*

Simulation in the field scale was conducted based on the reaction kinetics obtained from the core scale simulations. The aquifer model is a homogenous saline aquifer with dimensions of 10 km X 10 km X 50 m in the x, y, and z directions, respectively. The aquifer is 2500 m deep with a temperature of 163°F. The porosity is 0.15, horizontal permeability of 100 mD, and vertical permeability of 33 mD. The aquifer was initially at normal pore pressure gradient of 0.465 psi/ft (Dahle et al. 2009).

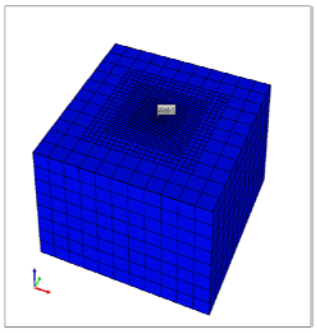

Property	Value
length	10 km
width	10 km
thickness	50 m
depth	2500 m
T	163°F
ϕ	0.15
k_h	100 mD
k_v	33 mD

FIG. 9 AQUIFER MODEL USED IN THE SIMULATION STUDY.

The aquifer was divided into Cartesian grids with 11X11X8 blocks in x, y, and z directions, with refining the grids into smaller blocks as we move toward the injector (Fig. 9). The injection well was completed at the center of the aquifer. Injection was conducted at a constant bottomhole pressure of 5740 psi (equivalent to a fracture pressure gradient of 0.7 psi/ft). The simulator ran for 30 years of CO_2 injection, and 1400 years after injection (the maximum number of time steps reached) to monitor the movement of CO_2 and the changes in trapping mechanisms. The aquifer was initially saturated with formation brine with the composition given in Table 4. WAG injection of CO_2 was conducted in each cycle which was composed of 9 months of CO_2 injection and 3 months of brine injection. Three brines were tested;

a) DI Water

b) Seawater without sulfate

c) Seawater

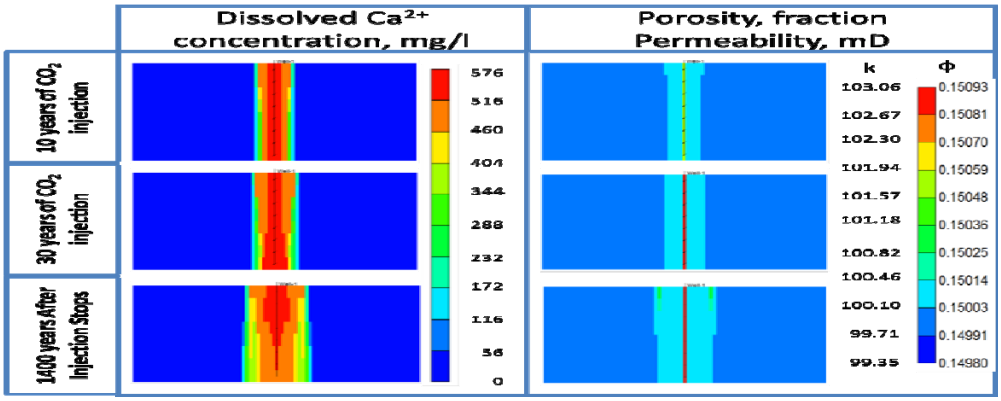

FIG. 10 DISTRIBUTION OF POROSITY, PERMEABILITY AND THE DISSOLVED CALCIUM IN THE AQUIFER AFTER 10 YEARS OF WAG INJECTION OF CO_2 AND DI WATER, AT THE END OF INJECTION, AND 1400 YEARS AFTER INJECTION STOPS.

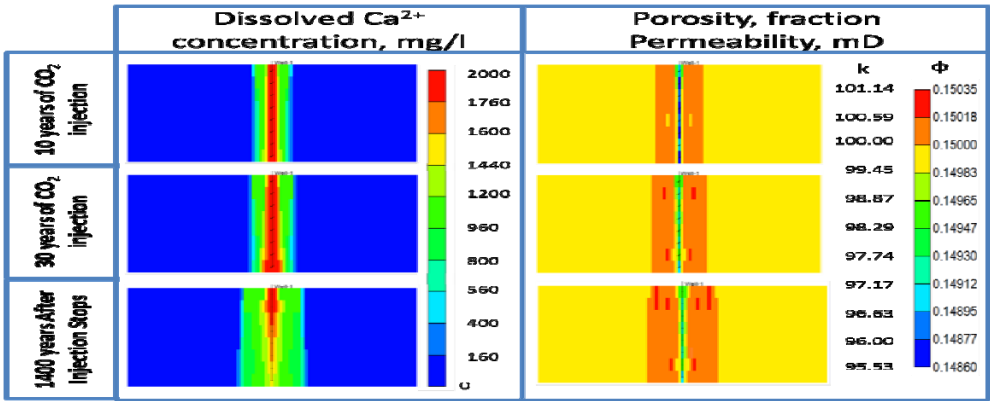

FIG. 11 DISTRIBUTION OF POROSITY, PERMEABILITY AND THE DISSOLVED CALCIUM IN THE AQUIFER AFTER 10 YEARS OF WAG INJECTION OF CO_2 AND SEAWATER WITHOUT SULFATE, AT THE END OF INJECTION, AND 1400 YEARS AFTER INJECTION STOPS.

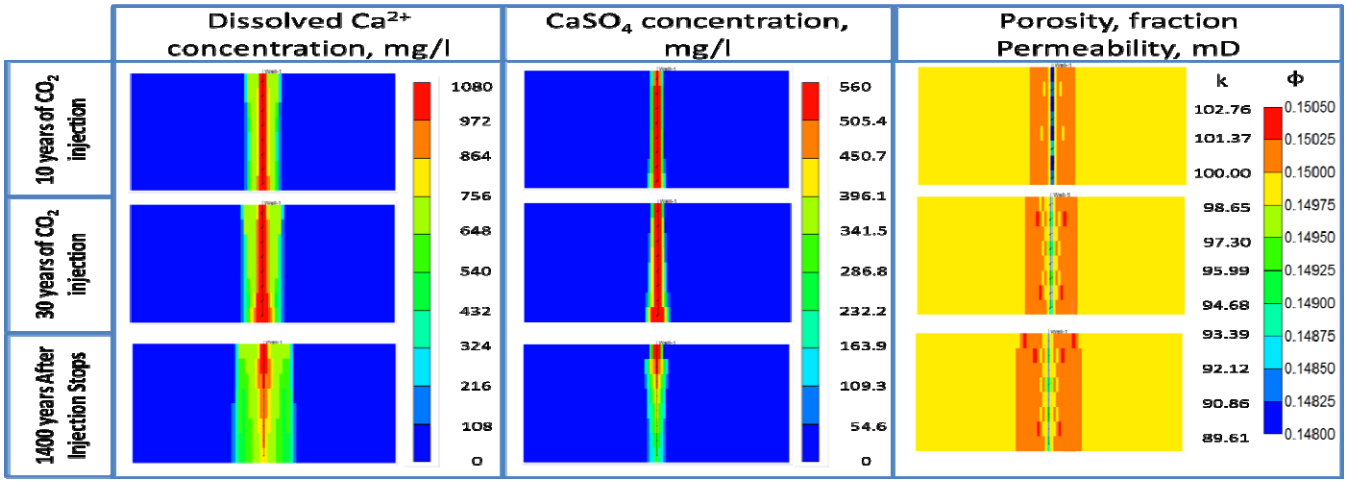

FIG. 12 DISTRIBUTION OF POROSITY, PERMEABILITY AND THE DISSOLVED CALCIUM IN THE AQUIFER AFTER 10 YEARS OF WAG INJECTION OF CO_2 AND SEAWATER, AT THE END OF INJECTION, AND 1400 YEARS AFTER INJECTION STOPS.

The amount of CO_2 injected for each case was almost the same. The cumulative CO_2 injected was 2.7 mega ton with 809,448 m^3 DI water for the first case, 2.63 mega ton with 794,844 m^3 seawater without sulfate for the second case, and 2.63 mega ton with 790,931 m^3 seawater for the third case. The values give a storage efficiency of 0.5% (total volume of CO_2 injected at reservoir conditions divided by the total pore volume of the aquifer, which equals 750,000,000 m^3).

The permeability and porosity distributions in the aquifer during WAG injection of CO_2 and 1400 years after injection stops are shown in Figs. 10-12. The dissolved calcium and calcium sulfate concentration (for the seawater case) are also shown in these figures. The main changes in the permeability occurred within the wellbore block grids, beyond these blocks a minor change in porosity and permeability was noted.

For the DI water case (Fig. 10) no damage was observed (no precipitation occurred). The dissolved calcium concentration shows that the maximum calcium concentration was 580 mg/l because of the small reaction rate constant (-9.2) as shown in Table 6. The maximum increase in the permeability was 3 mD around the wellbore region.

WAG injection of CO_2 and seawater without sulfate caused a 5 mD loss in the permeability around the wellbore (Fig. 11) after 10 years of injection due to the precipitation of calcium carbonate. At the end of injection (after 30 years) the damage reduced due to the rock dissolution, the final reduction in permeability was only 2 mD. The maximum dissolved calcium concentration was 2000 mg/l. The enhancement in permeability in the DI water case and damage in the seawater without sulfate case still insignificant, the change in permeability didn't exceed 5%.

More damage was observed in WAG injection of CO_2 with seawater, a 10 mD loss in permeability after 10 years of injection occurred, due to precipitation of calcium sulfate. Fig. 12 shows that the formation of

calcium sulfate occurred in this case and the calcium sulfate concentration increased to 560 mg/l.

Fig. 13 shows the contribution of each trapping mechanism to keep CO_2 in place over time. Table 7 shows that brine composition does not affect the trapping contribution of each trapping mechanism and the values are close for the three cases tested in this study.

Most of CO_2 was trapped as a free phase, and it contributes more than 40 mol% after 1400 years since the injection stopped. Fig. 13 shows that amount of free gases decreases with time, due to upward migration of CO_2 because of the gravity difference, leaving behind CO_2 trapped in residual phases; also more CO_2 is dissolved in the aquifer brine with time.

TABLE 7 TRAPPED PHASES AFTER WAG INJECTION OF CO_2 INTO SALINE CARBONATE AQUIFER

Brine Composition		DI Water	Seawater without Sulfate	Seawater
0 years after injection stops	Free CO_2 mol%	67.55	68.33	68.55
	Residual CO_2 mol%	15.94	15.23	15.48
	Dissolved CO_2 mol%	12.45	12.38	12.41
1400 years after injection stops	Free CO_2 mol%	42.91	43.77	43.73
	Residual CO_2 mol%	21.98	21.64	21.77
	Dissolved CO_2 mol%	34.47	33.90	34.05

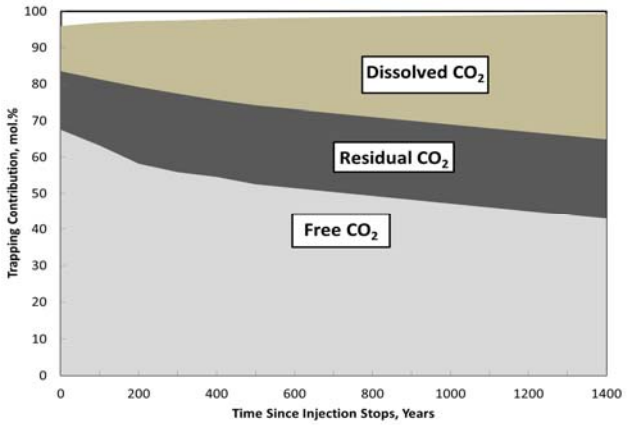

FIG. 13 TRAPPED PHASES AFTER WAG INJECTION OF CO_2 AND SEAWATER WITHOUT SULFATE INTO SALINE CARBONATE AQUIFER.

Conclusions

Brine composition is a critical factor that affects the chemical reactions between CO_2/brine/rock during CO_2 sequestration in carbonate aquifers. Different brine compositions, temperatures, and injection flow rates were examined. The study pertains mostly to limestone saline aquifers. A commercial reservoir simulator (CMG-GEM) was used to predict lab data and field results. Based on the results obtained, the following conclusions can be drawn:

1) Injection of lower salinity brines with CO_2 in WAG injection wells maintains the well injectivity and allows higher injection flow rate of CO_2 to be injected over time. The simulator predicted an enhancement in the permeability in the near wellbore region when DI water was injected with CO_2, while 5 mD reduction in the permeability in the near wellbore region was predicted when seawater without sulfate was injected with CO_2.
2) Using low sulfate brines is highly recommended in WAG injection projects to reduce the magnitude of damage in the near wellbore region. Up to 11 mD reduction in the permeability was noted when seawater was injected with CO_2.
3) Calcium chloride has the most significant effect on the limestone cores during sequestration, and increasing calcium chloride concentration caused a significant increase in calcium concentration in the core effluent samples.
4) A higher reaction rate constant ($\log(k_{25})$) was predicted as the brine salinity increased to simulate the increase in calcium concentration observed in the core effluent samples.
5) Based on the simulator results, the amount of CO_2 trapped in each trapping phase (free, residual, and dissolved) was almost the same regardless of the brine composition.

ACKNOWLEDGMENT

The authors would like to thank Texas Engineering Experiment Station (TEES) at Texas A&M University, Crisman Institute Petroleum Research for funding this work. Ms. K. Brady is acknowledged for proof reading this paper.

REFERENCES

Alkattan, M., Oelkers, E.H., Dandurand, J.L., Schott.J. 1998. An experimental study of calcite and limestone dissolution rates as a function of pH from -1 to 3 and temperature from 25 to 80°C. *Chemical Geology* **151**(1): 199–214.

Alotaibi, M.B., Nasralla, R.A., Nasr-El-Din, H.A., 2010. Wettability Challenges in Carbonate Reservoirs. Paper SPE 129972 presented at Improved Oil Recovery Symposium held in Tulsa, Oklahoma, 24-28 April.

Bacon, D.H., Sass, B.M., Bhargava, M., Sminchak, J. and Gupta, N. 2009. Reactive Transport Modeling of CO_2 and SO_2 Injection into Deep Saline Formations and Their Effect on the Hydraulic Properties of Host Rocks. *Energy Procedia* **1** (1) 3283–3290.

Bethke, C.M. 1996. Geochemical Reaction Modeling. Oxford University Press, New York.

Boving, T.B. and Grathwohl, P., 2001, Tracer diffusion coefficients in sedimentary rocks: correlation to porosity and hydraulic conductivity, *Journal of Contaminant Hydrology*, **53**(1): 85-100.

Cantucci, B., Montegrossi, G., Vaselli, O., Tassi, F., Quattrocchi, F., and Perkins E.H. 2009. Geochemical modeling of CO_2 storage in deep reservoirs: The Weyburn Project (Canada) case study. *Chemical Geology* **265** (1) 181–197.

Dahle, H.K., Eigestad, G.T., Nordbotten, J.M., and Pruess K. 2009. A Model-Oriented Benchmark Problem for CO_2 Storage. Workshop on Modeling and Risk of Assessment of Geological Storage of CO_2.

Duan, Z., Sun, R., Zhu, C., and Chou, I.M., 2006. An improved model for the calculation of CO_2 solubility in aqueous solutions containing Na^+, K^+, Ca^{2+}, Mg^{2+}, Cl^-, and SO_4^{2-}. *Marine Chemistry* **98** (2): 131–139.

Egermann, P., Bazin, B., and Vizika, O. 2005. An Experimental Investigation of Reaction-Transport Phenomena during CO_2 Injection. Paper SPE 93674 presented at the SPE Middle East Oil & Gas Show and Conference held in Bahrain, 12–15 March.

El-Khatib, N. 1995. Development of a Modified Capillary Pressure J-Function. Paper SPE 29890 presented at Middle East Oil Show, Bahrain, 11-14 March.

Enick, R.M., and Klara, S.M., 1989. CO_2 Solubility in Water and Brine Under Reservoir Conditions. *Chemical Engineering Communications* **90**(1): 23-33.

Flint, O., 1967. Increased Solubility of Calcium Sulphate in Sea Water Containing Hydrochloric Acid. *Desalination* **4**(3): 28-335.

Gaus, I., Azaroual, M., and Czernichowski-Lauriol, I. 2004. Reactive transport modeling of the impact of CO_2 injection on the clayey cap rock at Sleipner (North Sea). *Chemical Geology* **217** (3): 319– 337.

Grigg, R.B., and Svec, R.K., 2008. Injectivity Changes and CO_2 Retention for EOR and Sequestration Projects. Paper SPE 110760 presented at the SPE/DOE Improved Oil Recovery Symposium held in Tulsa, Oklahoma, U.S.A., 19-23 April.

Knauss, K.G., Johnson, J.W., and Steefel, C.I. 2005. Evaluation of the impact of CO_2, co-contaminant gas, aqueous fluid and reservoir rock interactions on the geologic sequestration of CO_2. *Chemical Geology* **217** (3): 339–350.

Krumhansl, J., Pawar, R., Grigg, R., Westrich, H., Warpinski1, N., Zhang, D., Jove-Colon1, C., Lichtner, P., Lorenz, J., Svec, R., Stubbs, B., Cooper, S., Bradley, C., Rutledge, J., and Byrer C., 2002. Geological Sequestration of Carbon Dioxide in a Depleted Oil Reservoir. Paper SPE 75256 presented at the SPE/DOE Improved Oil Recovery Symposium held in Tulsa, Oklahoma, 13–17 April.

Lee,Y.-J and Morse, J.W. 1999. Calcite precipitation in synthetic veins: Implications for the time and fluid volume necessary for vein filling. *Chemical Geology* **156** (1): 151–170.

Linnikov, O.D. and Podbereznyi, V.L., 1996. Prevention of sulfate scale formation in desalination of Aral Sea water. *Desalination* **105** (1): 143-150.

Marshall, W.L. and Slusher, R., 1968. Aqueous Systems at High Temperature. Solubility to 200°C of Calcium Sulfate and Its Hydrates in Seawater and Saline Water Concentrates, and Temperature-Concentration Limits. *J. Chem. Eng. Data* **13**(1); 83-93.

Meijer, J.A.M. and Van Rosmalen, G.M., 1984. Solubilities and Supersaturations of Calcium Sulfate and its Hydrates in Seawater. *Desalination*, **51** (3): 255-305.

Mohamed, I.M. and Nasr-El-Din, H.A. 2012. Permeability Alternation and Trapping Mechanisms during CO_2 Injection in Homogenous Limestone Aquifers: Lab and Simulation Studies. *Canadian Energy Technology and Innovation Journal* **1** (1):41-55.

Mohamed, I.M., and Nasr-El-Din, H.A. 2012. Formation Damage Due to CO_2 Sequestration in Deep Saline Aquifers. SPE 151142 presented at SPE International Symposium & Exhibition on Formation Damage Control held in Lafayeete, Louisiana, USA, 15–17 February.

Nighswander, J.A., Kaiogerakis, N., and Mehrotra, A.K., 1989. Solubilities of Carbon Dioxide in Water and 1 wt% NaCl Solution at Pressures up to 10 Mpa and Temperatures from 80 to 200°C. *J. Chem. Eng. Data* **34**(3): 355-360.

Partridge, E.P., and White, A.H., 1929. The Solubility of Calcium Sulfate from 0 to 200°, *J. Am. Chem. Soc*., **51**(2): 360-370.

Prutton, C.F., and Savage, R.L. 1945. The Solubility of Carbon Dioxide in Calcium Chloride-Water Solutions at 75, 100, 120° and High Pressures. *J. Am. Chem. Soc*. **67**(9): 1550–1554.

Raistrick, M., Hutcheon, I., Shevalier, M., Nightingale M., Johnson, G., Taylor, S., Mayer, B., Durocher, K., Perkins, E., and Gunter, B., 2009. Carbon dioxide-water-silicate mineral reactions enhance CO_2 storage; evidence from produced fluid measurements and geochemical modeling at the IEA Weyburn-Midale Project. *Energy Procedia* **1** (1): 3149–3155.

Shariat, A., Moore, R.G., Mehta, S.A., Van Fraassen, K.C., Newsham, K.E. and Rushing, J.A. 2012. Laboratory Measurements of CO_2-H_2O Interfacial Tension at HP/HT Conditions: Implications for CO_2 Sequestration in Deep Aquifers. Paper CMTC 150010 presented at the Carbon Management Technology Conference, Orlando, Florida, 7-9 February.

Sorensena, J.A., Holubnyaka, Y.I., Hawthornea, S.B., Millera, D.J., Eylandsa, K., Steadmana, E.N., and Harjua, J.A. 2009. Laboratory and numerical modeling of geochemical reactions in a reservoir used for CO_2 storage. *Chemical Geology* **265** (1):181-197.

Svensson, U., and Dreybrodt, W. 1992. Dissolution kinetics of natural calcite minerals in CO_2–water systems approaching calcite equilibrium. *Chemical Geology* **100**(1): 129-145.

Wellman, T.P., Grigg, R.B., McPherson, B.J., Svec, R.K., and Lichtner, P.C. 2003. Evaluation of CO_2-Brine-Reservoir Rock Interaction with Laboratory Flow Tests and Reactive Transport Modeling. Paper SPE 80228 presented at the SPE International Symposium on Oilfield Chemistry held in Houston, Texas, 5-7 February.

Wigand, M., Carey, J.W., Schütt, H., Spangenberg, E., and Erzinger, J. 2009. Geochemical effects of CO_2 sequestration in sandstones under simulated in situ conditions of deep saline aquifers. *Applied Geochemistry* **23** (9): 2735–2745.

Xu, T., Sonnenthal, E., Spycher, N., and Pruess, K. 2006. TOUGHREACT—A simulation program for non-isothermal multiphase reactive geochemical transport in variably saturated geologic media: Applications to geothermal injectivity and CO_2 geological sequestration. *Computers & Geosciences* **32** (2): 145–165.

Ibrahim M. Mohamed is a senior geomechanics engineer at Advantek International, Houston, Texas. He received his B.Sc. and M.Sc. degrees from the Petroleum Engineering Department at Cairo University, Egypt. And he received his PhD degree from Petroleum Engineering Department at Texas A&M University. His areas of research include well stimulation and formation damage removal, CO_2 injection, waste disposal and pressure transient analysis. He has published and presented more than 20 technical papers.

Jia He is a PhD candidate at Texas A&M University in petroleum engineering. Email: jia.he@pe.tamu.edu. His research interests include oil filed scale prediction and chemical treatments, CO_2 sequestration, cost effective acidizing treatments, and innovative acid fracturing studies. He has published several papers. He holds a BE degree from Eastern China University of Petroleum and MS degree from Texas A&M University, both in Petroleum Engineering.

Dr. Hisham A. Nasr-El-Din is a professor and holder of the John Edgar Holt Endowed Chair at Texas A&M University in Petroleum Engineering. Previously, he worked for 15 years as Principal Professional and Team Leader of the Stimulation Research and Technology Team, Saudi Aramco. Before joining Saudi Aramco, he worked for four years as a staff research engineer with the Petroleum Recovery Institute in Calgary. He also worked as a research associate with the University of Saskatchewan, the University of Ottawa and the University of Alberta, all in Canada. His research interests include well stimulation, formation damage, enhanced oil recovery, conformance control, interfacial properties, adsorption, rheology, cementing, drilling fluids, two-phase flow and non-damaging fluid technologies. Nasr-El-Din has several patents and has published and presented more than 480 technical papers. He has received numerous awards within Saudi Aramco for significant contributions in stimulation and treatment-fluid technologies and stimulation design, and for his work in training and mentoring. Nasr-El-Din holds B.Sc. and M.Sc. degrees from Cairo University, Egypt and a Ph.D. degree from the University of Saskatchewan, Canada, all in Chemical Engineering.